

# A one-dimensional temperature and age modeling study for selecting the drill site of the oldest ice core near Dome Fuji, Antarctica

Takashi Obase<sup>1</sup>, Ayako Abe-Ouchi<sup>1,2</sup>, Fuyuki Saito<sup>3</sup>, Shun Tsutaki<sup>2,4</sup>, Shuji Fujita<sup>2,4</sup>, Kenji Kawamura<sup>2,3,4</sup> and Hideaki Motoyama<sup>2,4</sup>

<sup>1</sup> Atmosphere and Ocean Research Institute, The University of Tokyo, Kashiwa, Japan

<sup>2</sup> National Institute of Polar Research, Research Organization of Information and Systems, Tachikawa, Japan

<sup>3</sup> Japan Agency for Marine-Earth Science and Technology (JAMSTEC), Yokosuka, Japan

<sup>4</sup> The Graduate University for Advanced Studies, SOKENDAI, Tachikawa, Japan

*Correspondence to:* Takashi Obase (obase@aori.u-tokyo.ac.jp)

**Abstract.** The recovery of a new Antarctic ice core spanning the past ~1.5 million years will advance our understanding of climate system dynamics during the Quaternary. Recently, glaciological field surveys have been conducted to select the most suitable core location near Dome Fuji (DF), Antarctica. Specifically, ground-based radar-echo soundings have been used to acquire highly detailed images of bedrock topography and internal ice layers. In this study, we use a one-dimensional (1-D) ice flow model to compute the temporal evolutions of age and temperature, in which the ice flow is linked with not only transient climate forcing associated with past glacial–interglacial cycles, but also transient basal melting diagnosed along the evolving temperature profile. We investigated the influence of ice thickness, accumulation rate, and geothermal heat flux on the age and temperature profiles. The model was constrained by the observed temperature and age profiles reconstructed from DF ice-core analysis. The results of sensitivity experiments indicate that ice thickness is the most crucial parameter influencing the computed age of the ice because it is critical to the history of basal temperature and basal melting, which can eliminate old ice. The 1-D model was applied to a 54 km-long transect in the vicinity of DF and compared with radargram data. We found that the basal age of the ice is mostly controlled by the local ice thickness, demonstrating the importance of high spatial resolution surveys of bedrock topography for selecting ice-core drilling sites.

## 1. Introduction

Earth’s climate system experienced glacial–interglacial cycles during the Quaternary, associated with the waxing and waning of continental ice sheets and climate system feedbacks (e.g., Shakun et al., 2015). Ice cores from the Antarctic ice sheet have provided fruitful information on past climate system changes because they can provide continuous reconstructions of ~~past~~ atmospheric compositions and temperature up to ~800 thousand years before the present (ka BP) (Jouzel et al., 2007; Kawamura et al., 2017). Such reconstructions have contributed to our understanding of the climate system dynamics of glacial–interglacial cycles (e.g., Abe-Ouchi et al., 2013; Obase et al., 2021). Meanwhile, a stacked sequence of marine sediments (Lisiecki and Raymo, 2005) indicates that the periodicity of glacial–interglacial cycles changed from 40 to 100 ka at the middle Pleistocene transition (MPT, approximately 800–1250 ka BP, Paillard, 2001; Clark et al., 2006). However, continuous ice core records that cover the MPT are still lacking, leading to a limited understanding of the mechanisms of this climate event. To help remedy this issue, the International Partnership for Ice Core Sciences (IPICS) has identified the quest for an “oldest ice core” as a critical scientific challenge. In this article, we define the term “old ice” as a continuous ice core with a basal age reaching 1.5 million years (Ma) BP, as defined in a IPICS community paper (Fischer et al., 2013).

In recent years, international efforts have been made to find plausible sites to obtain old ice in several locations in the interior of the Antarctic continent. In particular, in EPICA (European Project for Ice Coring in Antarctica) Dome C (EDC), glaciological surveys and ice-flow modeling

48 studies have been used to select the location of suitable sites (Parrenin et al., 2017; Young et al.,  
49 2017; Passalacqua et al., 2018; Lilien et al., 2021). The present article focuses on Dome Fuji (DF),  
50 Antarctica, which is located at 77.31° S, 39.70° E, with a surface elevation of 3810 m above sea level,  
51 and ice thickness of 3028 m. The most recent ice core at DF was obtained between 2003 and 2006  
52 (Motoyama et al., 2021). The ice age at the bottom of this core was approximately 720 ka BP based  
53 on Antarctic ice core chronology 2012 (AICC2012) (Kawamura et al., 2017; Uemura et al., 2018).  
54 The temperature of the ice was at the pressure-melting point near the bedrock (Motoyama et al.,  
55 2021). Recently, field surveys have been conducted to collect bedrock elevation data near DF using  
56 ground and airborne radar surveys. On the basis of surveys performed by Japanese Antarctic  
57 Research Expeditions (JARE) between the late 1980s and 2008, the results of which are included in  
58 BEDMAP\_2\_and\_3 datasets (Fretwell et al., 2013; [Frémand et al., 2022](#)), the typical ice thickness  
59 around DF is approximately 2000–3200 m (Fig. 1). Subsequently, the 54th JARE (2012–2013  
60 Antarctic summer) conducted ground-based radar surveys in areas where subglacial mountains were  
61 detected in the area south of DF (data compiled in Tsutaki et al., 2022). More recently, the Alfred  
62 Wegener Institute (AWI) in Germany conducted airborne radar surveys covering the DF area  
63 (Karlsson et al., 2018). On the basis of these data, the 59th and 60th JARE (2017–2018 and  
64 2018–2019 Antarctic summers) conducted ground-based radar surveys to investigate the internal  
65 [reflection horizons \(internal layers\) layers](#) of ice sheets over a distance of ~ 5650 km (Tsutaki et al.  
66 2022), covering the DF and NDF sites (the latter located at 77.8° S, 39.05° E, south of DF)  
67 (Rodríguez-Morales et al., 2020).

68 To select suitable ice-core drilling sites, the conditions that are required to preserve old ice  
69 using constraints from glaciological and climatological data should be investigated. Previous ice-  
70 flow modeling studies have examined the requirements to preserve old ice using both three-  
71 dimensional (3-D) and one-dimensional (1-D) models. Pattyn (2010) used a 3-D ice sheet model  
72 under present-day constant climate forcing, and suggested the importance of minimal horizontal flow  
73 and low geothermal heat flux (GHF) to preserve old ice near the base of ice sheets. Other studies  
74 have used 3-D models to represent 3-D ice-flow fields and ice age for the relatively small area near  
75 Antarctic Domes (Huybrechts et al., 2007; Seddik et al., 2011; Sun et al., 2014; Passalacqua et al.,  
76 2018; Zhao et al., 2018). These studies estimated the age distribution of the ice expected from 3-D  
77 ice flow fields under a constant present-day climate. More recent studies used glacial–interglacial  
78 cycle forcing (Sutter et al., 2019, 2021) and discussed how the past variation of the Antarctic ice  
79 sheet affects [ice-age distributions of ice](#).

80 One-dimensional vertical ice-flow models have been used [as-to estimate](#) the vertical profiles  
81 of age and temperature near Antarctic [Domesdomes](#), where horizontal flow is relatively minor.  
82 Horizontal surface velocity in the vicinity of DF and NDF is  $< 2 \text{ m a}^{-1}$ , and it has minor spatial  
83 variations, evidenced by satellite-based measurements (Rignot et al., 2011, 2017; Mougintot et al.,  
84 2012). Such 1-D models perform well in long-term forward simulations over glacial cycles and are  
85 able to conduct many simulations with different parameters. In particular, Fischer et al. (2013)  
86 investigated the influence of a wide range of parameters, including ice thickness, accumulation, and  
87 GHF on the basal age of ice. Their key finding was that melting at the base reduces the likelihood of  
88 old ice, and a lower ice thickness than that at previous ice core sites is a required condition to avoid  
89 basal melting. Furthermore, a lower accumulation rate generally contributes to increasing the age of  
90 the ice at a certain height from the bedrock but increases the chance of basal melting, owing to the  
91 reduced vertical advection of cold ice. Other studies used an equivalent 1-D ice-flow model,  
92 investigated the necessary conditions to keep the ice base frozen (Van Liefferinge and Pattyn, 2013;  
93 Van Liefferinge et al., 2018), and examined the observed basal conditions of the ice (Passalacqua et  
94 al., 2017). Parrenin et al. (2017) estimated ice-flow parameters and basal melting rate using internal  
95 layers of the ice near EDC and proposed candidate sites for old ice. [The reasonable resolution of ice  
96 core containing climate signals which can be analyzed with current methods is important.](#)  
97 [Particularly,](#) Saito et al. (2020) presented a numerical scheme of ice advection calculation [for an](#)

98 improved representation of annual layer thickness of the ice, and conducted numerical simulations  
99 using idealized glacial cycle forcings. ~~This contributed to a good representation of annual layer~~  
100 ~~thickness, which is critical to the occurrence of old ice near the base of an ice column.~~

101 Simplified factors in previous modeling studies were the time-dependent climate forcing and  
102 temperature profile, which are critical to basal ice melting. In particular, the basal temperature of the  
103 ice sheet shows a minimum during interglacials because it takes a long time to advect and diffuse  
104 surface temperature changes to the base of the ice sheet (Saito and Abe-Ouchi, 2004; Van  
105 Liefferinge et al., 2018). In this context, the model used in Parrenin et al. (2007) assumed that basal  
106 melting rates were constant over time, and Fischer et al. (2013) used pseudo steady-state assumption,  
107 i.e., a constant climate forcing. Parrenin et al. (2017) assumed that the temporal variations in basal  
108 melting rates are the same as accumulation rates. Some studies (Van Liefferinge and Pattyn, 2013;  
109 Passalacqua et al., 2017; Van Liefferinge et al., 2018) have investigated ice temperature using  
110 realistic climate forcing but did not investigate the resultant impact on the age of the ice. Similarly,  
111 Hondoh et al. (2002) and Talalay et al. (2021) estimated GHF at DF and other Antarctic domes based  
112 on observed vertical temperature profiles, but the observed age–depth profiles were not used as  
113 constraints. The ice thickness at Antarctic domes also changes with time, and can be up to 150 m  
114 thinner during glacial periods when surface mass balance (SMB) is reduced (Saito and Abe-Ouchi,  
115 2010).

116 Despite the close link between the temperature and age of ice owing to basal melting, the  
117 coupled simulations of thermodynamics and age of ice were not represented under transient climate  
118 forcing in previous modeling studies of old ice. In this study, we use a 1-D ice-flow model, which  
119 simultaneously computes the evolution of ice temperature and age, and the model is forced by past  
120 climate history. The remainder of the article is organized as follows: Section 2 describes the 1-D  
121 model used in this study. In Sect. 3, we apply this model to DF and conduct systematic sensitivity  
122 experiments to calibrate GHF and a tuning parameter of the vertical profile of ice velocity by  
123 comparing simulated age and temperature profiles with observations. We also use parameters at EDC  
124 to examine whether the model can simulate temperature and age profiles under different  
125 glaciological conditions. In Sect. 4, using the results of the tuned vertical velocity parameters, we  
126 investigate the influences of ice thickness, SMB, and GHF on the basal temperature and age. In Sect.  
127 5, we apply the 1-D model to the DF–NDF transect (over a distance of  $\sim 50$  km ) and compare the  
128 results with the internal layers of the ice.

## 129 2. Method

### 130 2.1. Model description

131 We used a 1-D ice-flow model, IcIES-2 (Saito et al., 2020). This model computes the  
132 temporal evolutions of the age and temperature profiles of ice columns.

133 The evolution of the age of the ice is computed using the vertical advection equation,  
134

$$135 \frac{\partial A}{\partial t} = -w \frac{\partial A}{\partial z} + 1, \quad (1)$$

136 where  $A$  is the age of the ice, defined as the duration since deposition, and  $w$  is the vertical velocity  
137 of the ice (a positive value indicates upward velocity). Here,  $\zeta$  is a normalized coordinate defined as  
138  $\zeta = \frac{z}{H}$ , where  ~~$s$  is the surface elevation~~,  $z$  is the height above bedrock, and  $H$  is the ice thickness (thus  
139  $\zeta = 1$  and  $0$  correspond to the ice surface and base, respectively). The first and second terms on the  
140 right-hand side of Equation (1) represent the vertical advection and aging owing to time-lapse,  
141 respectively.

142 The vertical velocity of the ice is assumed to be represented as:

$$143 w(\zeta) = - \left[ \left( M_s + M_b - \frac{\partial H}{\partial t} \right) \omega(\zeta) - M_b \right], \quad (2)$$

144 where the terms  $M_s$  and  $M_b$  represent surface (positive indicates ice gain) and basal (negative  
145 indicates ice melt) mass balance caused by accumulation and basal melting, respectively, and  $\frac{\partial H}{\partial t}$  is

146 the change in ice thickness over time. The normalized vertical velocity profile,  $\omega$ , is given as a  
 147 function of the normalized coordinate derived from Parrenin and Hindmarsh (2007), and Libby (1979):  
 148

$$149 \quad \omega(\zeta) = 1 - \frac{p+2}{p+1}(1 - \zeta) + \frac{1}{p+1}(1 - \zeta)^{p+2}, \quad (3)$$

150 where  $\omega$  is 1 at the surface and 0 at the base. Hence, in the case of steady state,  $\frac{\partial H}{\partial t} = 0$ , the vertical  
 151 velocity of the ice at the surface and base equates to  $-M_s$  and  $M_b$ , respectively. The shape of  $\omega$  with  
 152 different  $p$  parameters is demonstrated in Fig. 2, indicating that a larger  $p$ -value yields a larger  
 153 downward ice velocity. Compared with Fischer et al. (2013), who used a different formulation of the  
 154 vertical velocity profile with an  $m$  parameter (similar role as  $p$  of this study) of  $m = 0.5$  (Fig. 2  
 155 dashed lines),  $p = 3$  from Equation (3) gives a different vertical temperature profile, with a smaller  
 156 vertical velocity, particularly near the base of the ice.

157 The temperature of the ice is computed using the following vertical advection and diffusion  
 158 equation:

$$159 \quad \frac{\partial T}{\partial t} = -w \frac{\partial T}{\partial z} + \frac{1}{\rho_I c_p} \frac{\partial}{\partial z} \left( \kappa \frac{\partial T}{\partial z} \right), \quad (4)$$

160 where  $T$  is the temperature of the ice [K],  $\kappa$  is the thermal conductivity,  $\rho_I$  is the ice density, and  $c_p$  is  
 161 the heat capacity of the ice. The density of ice is set as a constant ( $910 \text{ kg m}^{-3}$ ), i.e., we ignore the  
 162 effects of lower density in the firn column. The strain heating term is neglected in the present study,  
 163 given that deformation of the ice would be minor near Antarctic domes because of very low  
 164 horizontal shear. The thermal conductivity and specific heat capacity of the ice are functions of  
 165 temperature (Greve and Blatter, 2009, following Ritz, 1987):

$$166 \quad \kappa = 9.828 e^{-0.0057T} \text{ W m}^{-1} \text{ K}^{-1}, \quad (5)$$

$$167 \quad c_p = (146.3 + 7.253T) \text{ J kg}^{-1} \text{ K}^{-1}, \quad (6)$$

168 Boundary conditions at the surface and base of the ice are required to close the equations. At  
 169 the ice surface, the age is set as 0, assuming no surface melt, and the temperature is set to the surface  
 170 temperature at the given time. The basal boundary conditions for temperature depend on the basal  
 171 condition:

$$172 \quad \frac{\partial T}{\partial z} \Big|_b = -\frac{G}{\kappa} \text{ if no melting,} \quad (7)$$

$$173 \quad T_b = T_{pm} \text{ if melting,} \quad (8)$$

174 where  $G$  is the geothermal heat flux (GHF) at the ice–bedrock boundary, and  $T_{pm}$  is the pressure-  
 175 melting point of the ice, which is given as a function of depth using a Clausius–Clapeyron gradient  
 176 ( $8.7 \times 10^{-4} \text{ K m}^{-1}$ ). The basal melting rate at the ice–bedrock interface is determined by the  
 177 conservation of heat:

$$178 \quad M_b \rho_I L = G - \kappa \frac{\partial T}{\partial z}, \quad (9)$$

179 where  $L$  is the latent heat of the ice ( $335 \text{ kJ kg}^{-1}$ ), and  $\frac{\partial T}{\partial z} \Big|_b$  is the temperature gradient at the  
 180 ice–bedrock interface. This model assumes basal melting only occurs at ice–bedrock interfaces, and  
 181 the temperature gradient at the ice–bedrock interface is calculated using a one-sided difference  
 182 discretization. The calculated basal melting rate  $M_b$  influences the velocity field according to  
 183 Equation (2). The model in the present study forecasts temperature in the bedrock, and thus the GHF  
 184 at the ice–bedrock interface has temporal variations. The bedrock is 3000 m thick divided vertically  
 185 into 17 equal layers; constant physical parameters are used for the bedrock (density =  $2700.0 \text{ kg m}^{-3}$ ,  
 186 heat capacity =  $1000.0 \text{ J kg}^{-1} \text{ K}^{-1}$ , and heat conductivity =  $3.0 \text{ W m}^{-1} \text{ K}^{-1}$ ), [used in Parizek and Alley](#)  
 187 [\(2004\)](#).

188 We adopted different vertical resolution setups in computations of the temperature and age  
 189 of the ice. The ice profile was discretized with 101 even vertical layers for thermodynamics; it was  
 190 discretized with 2661 unevenly spaced vertical layers (finer near the base to resolve the thin layers of  
 191 old ice) for age calculations, which was optimized following Saito et al. (2020). In the typical ice

192 column thickness of 3000 m near DF, the vertical resolution was set to approximately 20 m near the  
 193 surface and 20 cm near the bedrock, which is sufficient to resolve paleoclimate information  
 194 (glacial–interglacial annual layer variations) of ~1 ka. We used the rational function-based  
 195 constrained interpolation profile (RCIP) scheme in the advection equation for the numerical scheme,  
 196 as in Saito et al. (2020). One significant advantage of this scheme is the avoidance of numerical  
 197 diffusion and ability to reasonably preserve the time derivative of age, which is critical to the  
 198 resolution of old ice. We have tested the sensitivity to the vertical resolution of temperature  
 199 calculation and found that using fine vertical resolution leads to the formation of a temperature  
 200 inversion layer in the bottom of the ice, which can be a significant error in estimating basal  
 201 temperature gradient and basal melting. Therefore, we set the number of vertical layers of the model  
 202 for thermodynamics as 100 (each approximately 30 m thick) to prevent the representation of  
 203 temperature inversion layers. The time steps of the calculation of temperature and age were set to 20  
 204 years.

### 206 3. Model calibration using DF age and temperature profiles

#### 207 3.1. Experimental design

208 This section applies the 1-D model to DF under a realistic climate history for model  
 209 calibration and parameter constraint. Parrenin et al. (2007) determined the  $p$ -value as ~3.7 for DF,  
 210 but the chronology of ice older than 335 ka BP was not established at that time; therefore, we  
 211 revisited DF to determine the  $p$ -value covering the entire DF ice core age–depth dataset. The  
 212 glaciological boundary conditions at DF are summarized in Table 1: we used an ice thickness of  
 213 3028 m, a present-day SMB of 30 ice equivalent mm a<sup>-1</sup> (equivalent to 27.3 freshwater mm a<sup>-1</sup>,  
 214 based on Kameda et al., 2008 and Fujita et al., 2011), and a mean ice surface temperature at present  
 215 of -55.5 °C. We determined the boundary condition of ice surface temperature by calibrating the  
 216 temperature profile to be consistent with measured temperature profiles of the top 500 m of the ice,  
 217 within uncertainty ranges of the observations. The observed present-day 10-m-depth annual mean  
 218 snow temperature is -57.3 °C (Kameda et al., 1997), which was also used in Parrenin et al. (2007).  
 219 We note that the annual mean surface air temperature (SAT) based on meteorological observations  
 220 was -54.4 °C during the period 1995–1997 (Yamanouchi et al., 2003).

221 The model was forced by a realistic history of SAT and SMB. We used local SAT  
 222 anomalies at DF for the past 715 ka BP (Uemura et al., 2018) and the benthic record of marine  
 223 oxygen isotope data (Lisiecki and Raymo, 2005) to construct a continuous time series of SAT  
 224 anomalies during the last 2 Ma. We applied a simple translation of  $\delta^{18}\text{O}$  to scale the temperature  
 225 change at DF by the amplitude of glacial–interglacial cycles:

$$226 \Delta T_s = \alpha(\beta - \delta^{18}\text{O}), \quad (10)$$

227 where  $\delta^{18}\text{O}$  is the benthic marine oxygen isotope value [‰]; we set  $\alpha = 4.5$ , and  $\beta = 3.23$   
 228 to scale the amplitude of the glacial cycles, which generated a time series of temperature change over  
 229 the last 2 Ma, as shown in Fig. 3a. We used past SMB as a function of temperature anomaly  
 230 compared with the present day following Huybrechts and Oerlemans (1990), which is based on  
 231 saturation vapor pressure:

$$232 \underline{\text{aSMB}}(t) = \underline{\text{SMBa}}(\text{ref}) \cdot \exp\left\{22.47 \left[ \frac{T_0}{T_f(\text{ref})} - \frac{T_0}{T_f(t)} \right] \right\} \left\{ \frac{T_f(\text{ref})}{T_f(t)} \right\}^2, \quad (11)$$

233 where  $\underline{\text{SMBa}}(t)$  and  $\underline{\text{SMBa}}(\text{ref})$  represents past and present SMB rates, respectively.  $T_0 =$   
 234 273.16 K is the triple point of water, and  $T_f$  is the atmospheric temperature above the inversion layer  
 235 as a function of surface temperature ( $T_f[\text{K}] = 0.67T_s[\text{K}] + 88.9$ ). From this function, an increase in  
 236 surface air temperature of 1 °C increases SMB by approximately 7% (Fig. 3b). At the Last Glacial  
 237 Maximum (LGM, approximately 20 ka BP), when SAT was 8 °C cooler, the SMB was  
 238 approximately 60% of that of the present day, which is consistent with reconstructions based on the  
 239 isotopic content of the ice (Parrenin et al., 2016). This relationship between SAT and precipitation  
 240 changes used herein was within uncertainties estimated from observations and climate model

241 simulations, following a summary by IPCC AR6 (Chapter 9.4.2.3; Fox-Kemper et al., 2021), which  
 242 used the studies of Bracegirdle et al. (2020) and Frieler et al. (2015). Although this relationship is not  
 243 based on SMB, but rather on precipitation, herein we assume the precipitation change ratio is the  
 244 same as that of the SMB. The other boundary conditions (ice thickness and GHF) were set as  
 245 constants in the present study.

246 We used a result of transient simulation obtained by a 3-D ice sheet model ~~to simulate past~~  
 247 ~~ice thickness history; we used the 3-D ice sheet model~~ IcIES, which computes dynamics and  
 248 thermodynamics of ice sheets using the shallow-ice approximation to simulate past ice thickness  
 249 history. The experimental design was similar to that of Saito and Abe-Ouchi (2004, 2010) with some  
 250 changes; the domain of the 3-D model was the whole Antarctic continent, and the horizontal  
 251 resolution was set to 32 km. The spatial distribution of the GHF was from Martos et al. (2017). The  
 252 model was initialized using the present-day condition, and forced by the same temperature and SMB  
 253 changes as those of the 1-D model forcing for the past 2 Ma (Fig. 3a). The migrations of the  
 254 grounding lines were not forecasted, instead the positions of grounding lines were fixed to the  
 255 present day. We note that the advancement of grounding lines during glacial periods has a minor  
 256 impact on the ice thickness, in particular around the DF region, compared with the changes in  
 257 climate forcing (Saito et al., 2010). We extracted the history of changes in the ice thickness at DF  
 258 and EDC, which showed that the ice thickness was reduced by ~200 m during glacial periods, mainly  
 259 because of reduced SMB (Fig. 3c).

260 Using this set of boundary conditions, we conducted simulations with different GHFs  
 261 (50–70 mW m<sup>-2</sup>) to calibrate the model with observed values at the DF ice core. We used the  
 262 depth–age profile of the DF ice core, which was constructed by orbital tuning of a gas record above  
 263 ~2500 m, and by matching to the AICC2012 chronology below that depth (Kawamura et al., 2017).  
 264 We also used the measured depth–temperature profiles from the JARE54 surveys conducted during  
 265 the 2012–2013 Antarctic summer (Buizert et al., 2021). The model was initialized with the  
 266 conditions of 2 Ma BP, where the initial age and temperature were set to 0 years and –10 °C,  
 267 respectively, for the entire ice column. All experiments were integrated for 2 Ma to reach the present  
 268 day; therefore, the age of any ice older than 2 Ma did not appear in the experiments. These simplified  
 269 initial conditions generated unrealistic temperature fields in the early stage of the simulation, but  
 270 realistic glacial cycle forcing prevailed over the entire ice column within approximately 100 ka.  
 271 Therefore, we mainly analyzed the results of the last 1.5 Ma, which is sufficient to discuss old ice in  
 272 this study. Furthermore, we also applied this model to the conditions at EDC to check whether the  
 273 model could simulate the observed temperature and age profiles at this location (Table 1).

274 We also conducted three sensitivity experiments to investigate the impacts of the  $p$   
 275 parameters, uncertainty in the amplitude of past temperature changes, and inclusion of past ice  
 276 thickness changes, respectively. We found that  $p = 3$  gave one good age profile when compared with  
 277 the ice-core data; hence, we set  $p = 3$  as the reference in Sect. 3. The uncertainty in the past  
 278 temperature change was based on a study that proposed that the temperature change at the LGM in  
 279 interior regions of the East Antarctic ice sheet was less than previously estimated (Buizert et al.,  
 280 2021). We conducted a set of experiments where SAT anomalies were set to 0%, 25%, 50%, and  
 281 75% of the standard experiments, while keeping changes in SMB the same.

282

Parameters	DF	EDC
Ice thickness [m]	3028	3233
Surface mass balance <u>rate</u> [ice equivalent mm a <sup>-1</sup> ]	30.0	28.4
Surface temperature [°C]	–55.5	–54.65

283 **Table 1:** List of parameters used in Sect. 3. Ice thickness (DF and EDC), surface mass balance rate,  
 284 and surface temperature at EDC come from Parrenin et al. (2007); surface mass balance rate at DF  
 285 comes from Kameda et al. (2008) and Fujita et al. (2011); surface temperature at DF is calibrated in

286 this study and is within previously observed ranges (Kameda et al., 1997; Yamanouchi et al., 2003).

287

### 288 **3.2. Results for DF**

289 In Fig. 4, the simulated temperature profiles at 0 ka (end of the simulations) with different  
290 GHFs under the same  $p$ -value ( $p = 3$ ) are compared with observations (Fig. 4a). The close-up of the  
291 bottom 120 m of the ice column is shown in Fig. 4b; the basal temperature was well below melting  
292 point with a GHF of 54 and 56  $\text{mW m}^{-2}$ , and at the melting point with a GHF  $> 58 \text{ mW m}^{-2}$ .  
293 Compared with the observed temperature profile (Fig. 4, black lines), the simulated temperature near  
294 the ice base was colder by approximately 1 °C. In all simulations, the simulated temperature profiles  
295 were generally colder than observed temperature profiles, especially in the middle of the ice columns  
296 (Fig. 4a). The generally colder temperature of the ice may have several explanations. One is related  
297 to the pressure melting point of the ice. We used a pressure melting point of ice that depended only  
298 on local pressure, but there is also a dependence on the impurities and air content of the ice (e.g.,  
299 Parrenin et al., 2017; Passalacqua et al., 2017). A second explanation is related to the uncertainty in  
300 vertical velocity of the ice parameterized with  $p$  because a larger vertical advection contributes to a  
301 colder ice temperature.

302 The time series of simulated basal ice melting rates over the last 500 ka show that there have  
303 been significant temporal changes in these rates over time (Fig. 5a). With a GHF of 54  $\text{mW m}^{-2}$ , the  
304 temperature at the ice base has been below the melting point through the last 500 ka. In contrast, in  
305 the case of a GHF of 56  $\text{mW m}^{-2}$ , the basal melting rate is zero at 0 ka, while the maximum basal  
306 melting rate of 1  $\text{mm a}^{-1}$  occurs at the later stages of interglacial periods (e.g., 100 ka BP). This  
307 temporal variation in basal melting rate is caused by glacial-cycle forcing in SAT and SMB, and  
308 minimum basal melting tends to occur at the end of glacial periods as it lags SAT. This result is  
309 broadly consistent with previous studies (Saito and Abe-Ouchi, 2004; Van Liefferinge et al., 2018) in  
310 that colder ice, which accumulated during glacial maximums, advects towards the ice base owing to  
311 an increased SMB during interglacials. A larger GHF ( $\geq 60 \text{ mW m}^{-2}$ ) results in basal melting  
312 occurring most of the time, with an increase in basal melting rate of approximately 1  $\text{mm a}^{-1}$  for  
313 every 5  $\text{mW m}^{-2}$  increase in GHF.

314 The simulated age profiles at the present day are compared with the ice core-based profiles  
315 in Fig. 6a. With a small GHF (54  $\text{mW m}^{-2}$ ) where basal melting does not occur, the ice age at the  
316 ice–bedrock interface is  $> 1.5 \text{ Ma}$ . In contrast, if basal melting occurs, the ice age at the ice–bedrock  
317 interface can be much younger; for example, 761 or 620 ka for a GHF of 60 or 62  $\text{mW m}^{-2}$ ,  
318 respectively. The result obtained with a GHF of 60  $\text{mW m}^{-2}$  exhibits the closest fit to the data in  
319 terms of the age of ice at the base of the ice column. In this article, we define the “resolution of age”  
320 ( $\text{ka m}^{-1}$ ) as the inverse of annual layer thickness as an indicator of sufficient resolution for the  
321 chemical and isotopic contents of the ice (Lilien et al., 2021). In Fig. 6b, the resolution of old ice is  
322 compared with the actual DF ice core. The model results largely reproduced the glacial–interglacial  
323 contrasts in annual layer thickness caused by the temporal variations of SMB at this locality. The  
324 observed resolution of age was approximately 0.5–1  $\text{ka m}^{-1}$  near the base of the ice core, and the  
325 model results using a GHF of 60  $\text{mW m}^{-2}$  reproduced similar values. Furthermore, in a scenario with  
326 no significant basal melting, the annual layer thickness of 1.5 Ma BP ice is approximately 0.1 mm  
327 because 1.5 Ma ice appears directly above the bedrock (Fig. 6b, dark blue lines). In accordance with  
328 the results described above, a larger GHF tends to result in a higher basal melting rate and younger  
329 age of ice at the base of the column. One critical point is that an excessive GHF (i.e., an increase of  
330 the order of 2  $\text{mW m}^{-2}$ ) can have a considerable effect on the age of the ice and the likelihood of old  
331 ice.

332

### 333 **3.3. Results for EDC**

334 We also applied this model using the conditions at EDC to enable performance checks at an  
335 additional location. We used the parameters listed in Table 1 and conducted sensitivity experiments

336 with different GHFs. For the vertical velocity profile, we used  $p = 2.3$  following Parrenin et al.  
337 (2007). The model generally resulted in colder temperatures compared with observations, similar to  
338 that found at DF (Fig. 7). We note that the pressure melting point of the ice depended only on local  
339 pressure in Fig. 7, but several studies have considered the pressure melting point of the ice as a  
340 function of the pressure and air content of the ice, which has shown that the basal temperature is at  
341 the pressure melting point (Buizert et al., 2021). Modeling using a GHF of  $56 \text{ mW m}^{-2}$  gave a basal  
342 ice age of approximately 800 ka (Fig. 8a), which is similar to the value (802 ka) presented in Veres et  
343 al. (2013), and the resolution of age closely fits the chronology estimated from ice-core analysis (Fig.  
344 8b). One important result is that the threshold of GHF that allows basal melting is  $4 \text{ mW m}^{-2}$  lower at  
345 EDC compared with DF. This lower GHF can be attributed to the combination of larger ice thickness,  
346 smaller SMB, and higher SAT at the present day. The estimated GHF at EDC is smaller than that  
347 given by Parrenin et al. (2017), who estimated it to be  $60 \text{ mW m}^{-2}$ . This difference can be attributed  
348 to the difference in the history of basal melting, or the application of past climate history derived  
349 from DF to EDC. The results from the application of our model to EDC suggest that it may be  
350 applicable to different glaciological conditions, particularly different ice thicknesses and SMBs.

351

### 352 **3.4. Sensitivity to vertical velocity profiles, temperature amplitudes, and ice thickness changes**

353 Next, we evaluated the sensitivity of the temperature and age profiles to different vertical  
354 velocity profiles, temperature amplitudes, and ice thickness changes over glacial cycles. In Fig. 9,  
355 results using different  $p$ -values under an identical GHF ( $60 \text{ mW m}^{-2}$ ) are compared. A larger  $p$ -value  
356 induced a lower basal melting rate because of a larger vertical velocity and downward advection of  
357 cold ice from the surface, although this only had a minor impact on the temperature profile. The  
358 simulated age profiles indicate that a larger  $p$ -value induces a younger age of ice at mid-depths  
359 within the ice column (Fig. 9b), which is also a result of a larger vertical velocity. The age of the ice  
360 at the base of the column was approximately 800 ka BP in all five of the variable  $p$ -value simulations,  
361 partly because of the compensating effects of greater advection and less basal melting.

362 The results using DF conditions with different amplitudes of temperature change but constant  
363 GHF and  $p$  parameters (GHF =  $60 \text{ mW m}^{-2}$  and  $p = 3$ ) are summarized in Fig. 10. Here, we changed  
364 the  $\alpha$ -value in Equation 10 (1 is the control case). In the smallest amplitude experiment ( $\alpha = 0$ ), the  
365 temperature was set to the interglacial level and did not change in time. Note that the SMB variation  
366 was the same in all sensitivity experiments. The control experiments exhibited colder ice  
367 temperatures near the middle of the ice column compared with observations, and this cold bias was  
368 reduced when a smaller temperature amplitude over the glacial cycles was used (Fig. 10a), broadly  
369 consistent with Buizert et al. (2021). A smaller amplitude of the glacial cycle resulted in a younger  
370 age of ice at the bottom of the ice column (Fig. 10b) because of larger basal melting rates (Fig. 10c).  
371 This is because the mean temperature over the glacial cycles increases if the temperature amplitude  
372 of glacial–interglacial cycles is reduced. The results using a fixed surface temperature ( $dTs = 0.0$ )  
373 corresponded to the same present-day SAT for the last 2 Ma, which induced basal melting of  $\sim 1.5$   
374  $\text{mm a}^{-1}$  during most of this time. A slight fluctuation in basal melting still occurred owing to time-  
375 dependent SMB.

376 The results without ice thickness changes did not impact temperature profiles at the present-  
377 day (Fig. 11a), but impacted the history of basal melting (Fig. 11c). The mean basal melting rates at  
378 constant GHF can be reduced if ice thickness changes are included because the reduced ice thickness  
379 during glacial periods decreases the pressure-melting point. Moreover, the inclusion of ice thickness  
380 changes affects the phase of basal melting rates because it reflects the reduction in ice thickness and  
381 pressure-melting point at the base of the ice during glacials. The minimum in basal melting during  
382 the last glacial cycle occurs at the end of the LGM in the control experiment; in contrast, it occurs at  
383 the present-day in the no ice thickness change scenario. The absence of ice thickness changes results  
384 in larger mean basal melting rates and a younger age of ice at the base of the ice column (Fig. 11b).  
385 These results suggest that the basal melting rate in the past can be larger than the present-day rate.



386

387

### 3.5. Summary of Sect. 3

388

389

390

391

392

393

394

395

396

397

398

399

400

401

402

403

404

## 4. Sensitivity studies using various parameters around DF

405

### 4.1. Experimental design

406

407

408

409

410

411

412

This section investigates the impact of the three parameters, ice thickness, SMB, and GHF, which may have spatial variations in the DF region. We investigated a range of ice thicknesses between 2000 and 3200 m, based on an ice thickness map of the area around DF (Fig. 1). We used a present-day SMB range of 25–35 ice equivalent  $\text{mm a}^{-1}$ . There is large uncertainty in GHF; we adopted a range of 50–70  $\text{mW m}^{-2}$ . The list of experiments is given in Table 2. Other aspects of the experimental design are the same as in Sect. 3.

Variable	Parameter range
Ice thickness [m]	2000–3200, every 100
Present-day SMB <u>rate</u> [ice equivalent $\text{mm a}^{-1}$ ]	25–35, every 1
GHF [ $\text{mW m}^{-2}$ ]	50–70, every 2

413

Table 2: List of experiments in Sect. 4.

414

415

### 4.2. Results

416

417

418

419

420

421

422

423

424

425

426

427

428

429

430

431

In Fig. 12a, the relative effects of ice thickness and GHF on basal temperature are compared, using a constant SMB ( $30 \text{ mm a}^{-1}$ ). As in Sect. 3, we used an ice thickness of 3028 m, which is comparable to that at DF, and a GHF for basal melting of  $60 \text{ mW m}^{-2}$ . On the basis of the gradient of contours in Fig. 12a, an increase in ice thickness of 100 m has a comparable impact on the basal temperature as does an increase in GHF of  $2 \text{ mW m}^{-2}$ . In Fig. 12b, the relative effects of ice thickness and SMB are compared using a constant GHF ( $60 \text{ mW m}^{-2}$ ). A larger SMB results in a colder temperature; a 10% change in GHF leads to a  $\sim 4 \text{ }^\circ\text{C}$  change in the basal temperature, while a 10% change in SMB leads to a  $\sim 1 \text{ }^\circ\text{C}$  change. These results are generally consistent with those of Fischer et al. (2013), and suggest that the spatial distribution of SMB ( $\sim 20\%$  for the DF area) has a minor impact on the basal temperature compared with that of the ice thickness.

We further investigated the impact of different ice thicknesses on age profiles using the climatic conditions at DF (SMB =  $30 \text{ ice equivalent mm a}^{-1}$ ) and a calibrated GHF ( $60 \text{ mW m}^{-2}$ ). Figure 13a shows the simulated age of the ice at 50 and 100 m above the ice–bedrock interface, which were used as indicator depths for potential coring sites by Fischer et al. (2013). The results indicate that the rate of aging of ice decreases with ice thickness between 2800 and 3200 m owing to the occurrence of basal melting. Note that the age of 2 Ma BP is the limit of the experiments, and the

432 results indicate that the old ice exists 50 m above the bedrock if the ice thickness is thicker than  
433 ~2100 m. Figure 13b shows the age resolution of the 1.5 Ma BP ice, indicating that a larger ice  
434 thickness tends to show a finer age resolution. The vertical age profiles and resolution of ice ages at  
435 five selected ice thicknesses with constant GHF are shown in Fig. 14. According to Figure 14b, the  
436 expected age resolution of 1.5 Ma ice is approximately  $10 \text{ ka m}^{-1}$  with an ice thickness of 2800 m,  
437 and  $20 \text{ ka m}^{-1}$  with a smaller ice thickness of 2200 m.

## 439 5. Application to the DF–NDF transects

### 440 5.1. Experimental design

441 In this section, we apply the 1-D model to interpret the internal layers of the ice near DF  
442 under idealized boundary conditions. Here, we used the dataset from 17<sup>th</sup> December, 2017 obtained  
443 by ground surveys during JARE59 (2017–2018), which comprises a 54 km-long transect from DF to  
444 NDF (Fig. 1). The horizontal axis of Fig. 15 indicates the distance from DF, and the vertical axis  
445 indicates the depth from the surface. The gray shading indicates the reflectivity, which is an indicator  
446 of contours representing ice of the same age. The bedrock elevation, shown by brown lines, was  
447 detected based on the maximum reflectivity from the base (Tsutaki et al., 2022). The bedrock  
448 elevation was calibrated to match the observed bedrock elevation at DF. We calculated the 1-D age  
449 and temperature profiles of the ice at approximately 400 m intervals along the transect. We assumed  
450 that the vertical profile of vertical velocity could be determined locally, and that there were no  
451 horizontal interactions in temperature and age in this simulation. The present-day SMB was linearly  
452 interpolated between DF (30 ice equivalent  $\text{mm a}^{-1}$ ) and NDF (25.5 ice equivalent  $\text{mm a}^{-1}$ ). Note  
453 that the estimated SMB at NDF is 13% smaller than that at DF based on shallow ice cores (Oyabu et  
454 al., 2023). Because only very limited information on the spatial distribution of GHF is available, we  
455 set a uniform value of  $60 \text{ mW m}^{-2}$  following the discussion in Sect. 3. As described in Sect. 3, the  
456 initial age of the ice was set to 0, the temperature set to  $-10 \text{ }^\circ\text{C}$ , and the model was integrated over  
457 the last 2 Ma of forcing until it reached the present day (Fig. 3).

### 459 5.2. Results

460 In Fig. 15, the computed vertical profiles of the age are overlaid on a radargram using seven  
461 selected ages (colored lines), and the simulated basal temperature is indicated by shading in the  
462 bottom panel. The colored bar below the radargram indicates the simulated present-day basal  
463 temperature. The simulated distribution of ice age captured large-scale features in the black–white  
464 contour lines derived from the radargram signal (grayscale color in Fig. 15). The simulated age  
465 contours of 21 ka BP (approximately 500 m depth) and 128 ka BP (approximately 1500 m depth) can  
466 be traced from DF, although the deepest layer-horizon corresponding to an age older than 300 ka BP  
467 is hard to see in this image. Where ice is relatively thick (e.g., 20–25 km from DF), the simulated age  
468 of the ice at the ice–bedrock interface is younger than 700 ka BP, while ice older than 1.5 Ma BP  
469 occurs where the ice is relatively thin. On the basis of the results shown in Fig. 13b, we note that thin  
470 ice gives a poorer age resolution for the old ice. A comparison of the simulated ice age and  
471 radargram signal gives an opportunity to examine the validity of the model results. For example,  
472 between 5 and 35 km from DF, the computed 128 ka BP contour deviates to shallower levels (by 150  
473 m) compared with the tracked layer-horizon for the age obtained from the radar measurements,  
474 suggesting that the model overestimates the age of the ice near the bedrock in such locations.

## 476 6. Discussion

477 In this study, we used a 1-D ice-flow model, which computes the temporal evolution of age  
478 and temperature profiles. We used glaciological conditions at DF to tune some unknown parameters  
479 according to the observed temperature and age profiles. The results showed that the age profile is  
480 sensitive to the choice of GHF, but one experiment using a specific combination of GHF and vertical  
481 velocity profile exhibited reasonable temperature and age profiles (Figs 4 and 6). One important

482 result is that the melting rate at the base of the ice exhibits temporal changes associated with  
483 glacial–interglacial forcing. This is caused by relatively cold ice deposited during glacial periods  
484 being pushed towards the bottom of the ice column by increased SMB and downward advection  
485 during interglacial periods, as shown in previous studies (e.g., Van Liefferinge et al., 2018). This  
486 point is critical for preserving old ice because basal melting rates during past interglacials can be  
487 higher than that of the present day (Fig. 5). Our sensitivity experiments highlighted the relative  
488 effects of ice thickness and GHF, whereby a small GHF excess above the condition that induces  
489 basal melting can result in a considerable reduction in the age of ice at the ice–bedrock interface (Fig.  
490 6a). Below, we discuss the limitations of the interpretations of our results, their relevance to previous  
491 ice-flow modeling studies, and uncertainty factors.

492 On the basis of data presented in Fig. 6, a GHF of  $60 \text{ mW m}^{-2}$  sufficiently explains the  
493 observed temperature and age–depth profiles of the DF ice core. However, there is considerable  
494 uncertainty in the estimation of the actual GHF value at DF because of some simplifications in the  
495 model experiments and limited representations in physics. One point of difference is that the model  
496 tends to give a generally colder temperature profile compared with the observations (Fig. 4), which  
497 suggests that the model overestimates the GHF threshold of basal freezing. One possible reason for  
498 this difference is that the basal melting of ice can occur within a certain ice thickness; the  
499 extrapolation of observed temperature profiles at DF and EDC (Figs 4 and 7, black lines) shows that  
500 the ice reaches the pressure-melting point approximately 30 m above the bedrock. This feature  
501 cannot be simulated in the model of the present study, which assumes that basal melting can only  
502 occur at the ice–bedrock interface. These representations in the physics of basal melting can be  
503 improved by using enthalpy as a state variable and adopting polythermal ice sheet models (e.g.,  
504 Aschwanden et al., 2012). There is also uncertainty in the parameterization of the conductivity and  
505 heat capacity of the ice. We use these parameters as a function of temperature, but they can depend  
506 on the fabric of the ice, which makes it challenging to estimate them. Hence, these physical  
507 parameters can be a source of uncertainty in estimating GHF, and can be a source of difference from  
508 other studies. Another important factor in the temperature profiles is the temperature anomaly over  
509 glacial cycles, as a smaller glacial–interglacial temperature change tends to result in a warmer, more  
510 linear temperature profile compared with the control experiment (Fig. 10a). The surface air  
511 temperature change over the last glacial cycle used in this study is based on deuterium and oxygen  
512 isotopes (Uemura et al., 2018), which exhibit an LGM temperature anomaly of approximately  $8 \text{ }^\circ\text{C}$   
513 (Fig. 3a). A recent study proposed that the temperature anomaly at the LGM at DF and EDC was  
514 approximately half of previous estimates based on the observed temperature profiles and other  
515 independent methods (Buizert et al., 2021). This study is in agreement with Buizert et al. (2021) in  
516 that our control experiment exhibits colder ice temperatures, especially at mid-depth within the ice  
517 column, and a smaller temperature difference between glacial and interglacial periods improves the  
518 modeled temperature profiles (Fig. 10a). If this is indeed the case, the actual threshold of the GHF  
519 value for basal freezing should be lower than that used in the control experiment. We also found that  
520 if the temperature anomaly is half that of the control case, a GHF smaller than the control value ( $58$   
521  $\text{mW m}^{-2}$ ) gives the closest age profile. We investigated the sensitivity to ice thickness as in Fig. 13,  
522 and obtained comparable results in terms of the age near the bottom of the ice column (not shown).  
523 These results indicate that several uncertainties (e.g., climate forcing and vertical velocity) can affect  
524 the temperature and age profiles under a certain condition, but if we calibrate the GHF with the DF  
525 ice-core age profile as in Sect. 3, we obtain comparable results regarding the sensitivity to ice  
526 thickness.

527 We note that the simulated age of the ice depends on the shape of the vertical velocity profile  
528 of the ice. The formulation of the present study uses a smaller vertical ice velocity, especially near  
529 the base, compared with that used in Fischer et al. (2013). Because the age of the ice is related to the  
530 inverse of the vertical velocity, a different vertical velocity profile or  $p$  parameter can lead to a  
531 quantitatively different result. Moreover, vertical velocity profiles represented by a single  $p$ -value are

532 merely one assumption; this formulation is derived from a solution of an idealized ice-sheet  
533 configuration (Lliboutry, 1979), which may not be the case for realistic ice sheets. For example, the  
534 observed magnitude of layer thinning of the DF ice core exhibits a decreasing trend over the bottom  
535 500 m (Fig. 6). According to analyses of the DF ice core (Azuma et al., 1999; Saruya et al., 2022) or  
536 3-D ice sheet modeling (Seddik et al., 2011), deformation of the ice or flow regime towards the  
537 bottom of the ice is complex, suggesting parameterizing vertical velocities is difficult particularly  
538 near ice bottom. Improving velocity fields in ice sheet model would be an important issue for future  
539 studies. Thus, we suggest that both horizontal and vertical ice flow should be complex, which may be  
540 difficult to represent using the current formulation of vertical velocity profiles.

541 We also note that the resolution of 1.5 Ma ice, ~~one indicator of old ice~~, depends on ice  
542 thickness. In particular, Lilien et al. (2021) presented similar 1-D ice-flow model results from  
543 BELDC (Beyond EPICA Little Dome C, ice thickness of ~~~2750–2765~~ m) constrained by radar-  
544 imaged internal layers and estimated the resolution of 1.5 Ma ice as  $19 \pm 2$  ka m<sup>-1</sup>. ~~In contrast, o~~Our  
545 results for EDC conditions (with a small enough GHF to keep the base of the ice frozen) have an ice  
546 age resolution of approximately 10 ka m<sup>-1</sup> (Fig. 8, dark blue lines), which is approximately half that  
547 of Lilien et al. (2021). This difference can be attributed to the combination of model parameters, such  
548 as ice thickness,  $p$  of the vertical velocity profile, or SMB history (3233 m and  $p = 2.3$  in this study),  
549 because the two studies adopted the same formulation of the vertical velocity profile. According to  
550 Figs. 13 and 14, a larger ice thickness leads to a better resolution of the ice age if the base of the ice  
551 remains frozen throughout time. It is worth mentioning that the approach in ice thickness are  
552 different between Lilien et al. (2021) which used ice thickness of 2765 m, including a thickness of a  
553 basal unit of ~200 m and thus an effective ice thickness of 2565 m. Therefore, the different effective  
554 ice thickness (3233 m for EDC) would be the most critical factor in-for the difference in-of the age  
555 resolution of 1.5 Ma ice when compared with Lilien et al. (2021), who used BELDC conditions-(ice  
556 thickness of 2750 m).

557 Application of the 1-D model to the transect between DF and NDF provides an opportunity to  
558 examine the influence of spatially varying glaciological conditions (e.g., ice thickness and GHF) on  
559 the age of the ice. The simulated age–depth distributions with constant GHF but different ice  
560 thickness and SMB exhibit general agreement with observed internal ~~layers-horizons~~ (Fig. 15). One  
561 noticeable model–data discrepancy occurs at 14–18 km from DF, where the simulated age contours  
562 of 128 ka BP are ~150 m above the ~~observed internal isochrone horizonslayers~~ traced from DF. This  
563 model–data discrepancy indicates that the effects of vertical or horizontal advection (Huybrechts et  
564 al., 2007; Sutter et al., 2021), or spatial distribution-variation of GHF may have contributed to this  
565 difference. Although the relative importance of the spatial distributions of GHF, SMB, and  
566 horizontal flow is difficult to assess in the present study, we expect that future glaciological data  
567 constraints and model developments will better constrain these uncertain parameters and the spatial  
568 distribution of old ice. One recently published present-day SMB from the vicinity of the DF region  
569 exhibits spatial variabilities reflecting surface topographical features (Van Liefferinge et al., 2021).  
570 On the basis of systematic sensitivity experiments (Sect. 4), we have shown that the impact of SMB  
571 on the age of the ice is relatively minor compared with that of ice thickness, but the small-scale  
572 features present in internal reflection horizonslayers of the ice can be improved by using the spatial  
573 distribution of present-day SMB, and this will contribute to the selection of the most suitable drilling  
574 site.

## 576 7. Conclusions

577 We draw the following conclusions from this study:-

- 578 1. In experiments using the DF configuration, the model largely reproduced the observed age and  
579 temperature profiles under a calibrated GHF. If the GHF is small enough to keep the basal  
580 temperature below the melting point, it is expected that ~1.5 Ma ice could be present. According  
581 to Figs. 14 and 15, the simulated annual layer thickness of ~1.5 Ma ice is approximately 0.05 to

582 0.1 mm, which corresponds to 10 to 20 ka m<sup>-1</sup>. According to IPICS, this is a feasible resolution  
583 for analysis with minimized effects of diffusion. This is also true for EDC, but the threshold of  
584 GHF for basal melting is different because of a different ice thickness and SMB.

- 585 2. Under the configuration and range of parameters of the present study, the ice thickness has a  
586 larger impact on basal melting than does the present-day SMB; an ice thickness difference of  
587 ~100 m corresponds to an SMB difference of 5 ice equivalent mm a<sup>-1</sup> (Fig. 12). Near the DF  
588 region, the ice thickness exceeds such a spatial variability, while SMB does not. Although there  
589 is considerable uncertainty in the spatial distribution of GHF, ice thickness is suggested to be  
590 one of the most critical factors for the preservation of old ice.
- 591 3. The calibrated GHF in this study, which is based on an ice-core age profile, has uncertainties.  
592 The basal melting rate, which is critical to the age of ice near the bottom of the column, is  
593 determined by the thermal conditions. The basal melting exhibits temporal variability as a result  
594 of glacial–interglacial changes in climate, and the maximum basal melting tends to occur at the  
595 end of interglacials. Thus, the basal melting is influenced by climate forcing of past temperature  
596 and ice thickness changes, which have uncertainties. Furthermore, a vertical velocity profile  
597 parameterized with a uniform *p*-value can be a source of uncertainty, and may have a limited  
598 ability to represent complex ice flow near the bottom of the ice column.
- 599 4. From the simulation of the DF–NDF transect, a small ice thickness and colder basal temperature  
600 are the necessary conditions for the presence of old (~1.5 Ma) ice. However, a small ice  
601 thickness contributes to a coarser resolution of the old ice (small annual layer thickness), which  
602 may make it difficult to extract paleoclimate information on glacial-interglacial times scales. As  
603 discussed in Pattyn (2010), ice thickness is found to be a compromising factor in the selection of  
604 a drilling site.
- 605 5. The simulation along the DF–NDF transect does not reproduce the depth of the internal layers of  
606 the ice corresponding to 128 ka BP at some locations (e.g., at distances 5–35 km from DF),  
607 suggesting a possible error in the simulated age of ice near the bottom of the ice column. The  
608 simulated age of ice in this area, especially where there is a large discrepancy between the  
609 simulation and radar images, could be caused by uncertainties derived from several assumptions  
610 or uncertainty in the model or methods, including spatial distributions of GHF, representation in  
611 vertical temperature profile that depends only on normalized altitude–height (DF ice core  
612 suggests complex ice-flow near its base), representation in thermodynamics associated with  
613 basal melting, or history of surface temperature changes. Therefore, future improvements in  
614 numerical models and methods would contribute to better constraining the age of the ice.

615 A recent compilation of ice thickness data around DF indicates the presence of complex and steep  
616 terrain in the area, with uncertainty in bedrock elevation of > 60 m (Tsutaki et al., 2022),  
617 highlighting the necessity of a high-spatial-resolution survey of bedrock topography. The results  
618 from this study help to support the interpretation of observational data and the selection of a suitable  
619 drilling site.

#### 620 **Code availability:**

621 The numerical model is available from Github. <https://github.com/saitofuyuki/icies2.git>

#### 622 **Data availability:**

623 The scripts and data for conducting experiments and analyzing results are available at AORI-CESD  
624 (<https://cesd.aori.u-tokyo.ac.jp/cesddb/publication/index.html>). All figures were generated using  
625 GMT version 4.5.9. The ice core chronology and temperature at DF are available from previously  
626 published articles (Veres et al., 2013; Kawamura et al., 2017; Buizert et al., 2021).

#### 627 **Author contribution**

631 T. O., A. A-O., and F. S. conceived the study, developed the numerical model, designed and carried  
632 out the experiments, and analyzed the results. T. S., S. F., K. K., and H. M. provided glaciological  
633 data from JARE surveys and contributed to the experimental design. T. O. prepared the manuscript  
634 with contributions from all co-authors.

635

### 636 **Competing interests**

637 The authors declare that they have no conflict of interest.

638

### 639 **Acknowledgments**

640 We would like to thank Frédéric Parrenin and two anonymous referees for their valuable comments,  
641 which have substantially improved our manuscript. We thank Kenichi Matsuoka, Brice Van  
642 Liefferinge, and Ralf Greve for their fruitful discussions. This research was supported by JSPS  
643 Kakenhi JP17H06104, JP17H06323, and JP18H05294. T. O., A. A-O., and F. S. were supported by  
644 JPJSBP120213203. F. S. was also supported by JSPS Kakenhi JP17K05664. [The 3-d ice sheet model  
645 simulations were performed on the Earth Simulator 4 at Japan Agency for Marine-Earth Science and  
646 Technology \(JAMSTEC\).](#) We thank David Wacey, PhD, from Edanz (<https://jp.edanz.com/ac>) for  
647 editing a draft of this manuscript.

648

### 649 **References**

- 650 1. Abe-Ouchi, A., Saito, F., Kawamura, K., Raymo, M. E., Okuno, J., Takahashi, K., and Blatter,  
651 H.. Insolation-driven 100,000-year glacial cycles and hysteresis of ice-sheet volume. *Nature* 500,  
652 190–193, doi: 10.1038/nature12374, 2013
- 653 2. Aschwanden, A., Bueller, E., Khroulev, C., and Blatter, H.: An enthalpy formulation for glaciers  
654 and ice sheets, *J. Glaciol.*, 58, 441–457, doi:10.3189/2012JoG11J088, 2012.
- 655 3. Azuma, N., Wang, Y., Mori, K., Narita, H., Hondoh, T., Shoji, H., and Watanabe O.: Textures  
656 and fabrics in the Dome F (Antarctica) ice core, *Ann. Glaciol.*, 29, 163–168,  
657 <https://doi.org/10.3189/172756499781821148>, 1999.
- 658 4. Bracegirdle, T. J., Krinner, G., Tonelli, M., et al. Twenty first century changes in Antarctic and  
659 Southern Ocean surface climate in CMIP6. *Atmos Sci Lett.*, doi: 10.1002/asl.984, 2020
- 660 5. Burton-Johnson, A., Dziadek, R., and Martin, C., Geothermal heat flow in Antarctica: current  
661 and future directions, *The Cryosphere*, 14, 3843–3873, doi:10.5194/tc-14-3843-2020, 2020
- 662 6. Buizert, C., Fudge, T. J., Roberts, W. H., Steig, E. J., Sherriff-Tadano, S., Ritz, C., Lefebvre, E.,  
663 Edwards, J., Kawamura, K., Oyabu, I., and Motoyama, H. et al.: Antarctic surface temperature  
664 and elevation during the Last Glacial Maximum, *Science* 372(6546), 1097–1101, doi:  
665 10.1126/science.abd2897, 2021
- 666 7. Carson, C. J., McLaren, S., Roberts, J. L., Boger, S. D., and Blankenship, D. D.: Blankenship,  
667 hot rocks in a cold place: High sub-glacial heat flow in East Antarctica, *J. Geol. Soc. London*,  
668 171, 9–12, <https://doi.org/10.1144/jgs2013-030>, 2014.
- 669 8. Clark, P., Archer, D., Pollard, D., Blum, J. D., Rial, J. A., Brovkin, V., Mix, A. C., Pisias, N. G.  
670 and Roy, M.: The middle Pleistocene transition: characteristics, mechanisms, and implications  
671 for long-term changes in atmospheric pCO<sub>2</sub>, *Quaternary Science Reviews*, 25, 23–24, 3150–  
672 3184. doi: 10.1016/j.quascirev.2006.07.008, 2006
- 673 9. Fischer, H., Severinghaus, J., Brook, E., Wolff, E., Albert, M., Alemany, O., Arthern, R.,  
674 Bentley, C., Blankenship, D., Chappellaz, J., Creyts, T., Dahl-Jensen, D., Dinn, M., Frezzotti,  
675 M., Fujita, S., Gallee, H., Hindmarsh, R., Hudspeth, D., Jugie, G., Kawamura, K., Lipenkov, V.,  
676 Miller, H., Mulvaney, R., Parrenin, F., Pattyn, F., Ritz, C., Schwander, J., Steinhage, D., van  
677 Ommen, T., and Wilhelms, F.: Where to find 1.5 million yr old ice for the IPICS “Oldest-Ice”  
678 ice core, *Clim. Past*, 9, 2489–2505, doi:10.5194/cp-9-2489-2013, 2013.
- 679 10. Fox-Kemper, B., H. T. Hewitt, C. Xiao, G. Adalgeirsdottir, S. S. Drijfhout, T. L. Edwards, N. R.  
680 Golledge, M. Hemer, R. E. Kopp, G. Krinner, A. Mix, D. Notz, S. Nowicki, I. S. Nurhati, L.

- 681 Ruiz, J-B. Sallee, A. B. A. Slangen, Y. Yu: Ocean, Cryosphere and Sea Level Change. In:  
682 Climate Change 2021: The Physical Science Basis. Contribution of Working Group I to the  
683 Sixth Assessment Report of the Intergovernmental Panel on Climate Change [Masson-Delmotte,  
684 V., P. Zhai, A. Pirani, S. L. Connors, C. Pean, S. Berger, N. Caud, Y. Chen, L. Goldfarb, M. I.  
685 Gomis, M. Huang, K. Leitzell, E. Lonnoy, J.B.R. Matthews, T. K. Maycock, T. Waterfield, O.  
686 Yelekci, R. Yu and B. Zhou (eds.)]. Cambridge University Press, 2021.
- 687 11. Frieler, K., Clark, P., He, F. et al. Consistent evidence of increasing Antarctic accumulation with  
688 warming. *Nature Clim Change* 5, 348–352. doi: 10.1038/nclimate2574, 2015.
- 689 ~~11.~~12. Frémand, A. C., Fretwell, P., Bodart, J., Pritchard, H. D., Aitken, A., Bamber, J. L., Bell, R.,  
690 Bianchi, C., Bingham, R. G., Blankenship, D. D., Casassa, G., Catania, G., Christianson, K.,  
691 Conway, H., Corr, H. F. J., Cui, X., Damaske, D., Damm, V., Drews, R., Eagles, G., Eisen, O.,  
692 Eisermann, H., Ferraccioli, F., Field, E., Forsberg, R., Franke, S., Fujita, S., Gim, Y., Goel, V.,  
693 Gogineni, S. P., Greenbaum, J., Hills, B., Hindmarsh, R. C. A., Holmlund, P., Holschuh, N.,  
694 Holt, J. W., Humbert, A., Jacobel, R. W., Jansen, D., Jenkins, A., Jokat, W., Jordan, T., King, E.,  
695 Kohler, J., Krabill, W., Langley, K., Lee, J., Leitchenkov, G., Leuschen, C., Luyendyk, B.,  
696 MacGregor, J., MacKie, E., Matsuoka, K., Morlinghem, M., Mouginit, J., Nitsche, F. O., Nogi,  
697 Y., Nost, O. A., Paden, J., Pattyn, F., Popov, S. V., Riger-Kusk, M., Rignot, E., Rippin, D. M.,  
698 Rivera, A., Roberts, J., Ross, N., Ruppel, A., Schroeder, D. M., Siegert, M. J., Smith, A. M.,  
699 Steinhage, D., Studinger, M., Sun, B., Tabacco, I., Tinto, K., Urbini, S., Vaughan, D., Welch, B.  
700 C., Wilson, D. S., Young, D. A., and Zirizzotti, A.: Antarctic Bedmap data: FAIR sharing of 60  
701 years of ice bed, surface and thickness data, *Earth Syst. Sci. Data Discuss.* [preprint],  
702 <https://doi.org/10.5194/essd-2022-355>, in review, 2022.
- 703 ~~12.~~13. Fretwell, P., Pritchard, H. D., Vaughan, D. G., Bamber, J. L., Barrand, N. E., Bell, R.,  
704 Bianchi, C., Bingham, R. G., Blankenship, D. D., Casassa, G., Catania, G., Callens, D., Conway,  
705 H., Cook, A. J., Corr, H. F. J., Damaske, D., Damm, V., Ferraccioli, F., Forsberg, R., Fujita, S.,  
706 Gim, Y., Gogineni, P., Griggs, J. A., Hindmarsh, R. C. A., Holmlund, P., Holt, J. W., Jacobel, R.  
707 W., Jenkins, A., Jokat, W., Jordan, T., King, E. C., Kohler, J., Krabill, W., Riger-Kusk, M.,  
708 Langley, K. A., Leitchenkov, G., Leuschen, C., Luyendyk, B. P., Matsuoka, K., Mouginit, J.,  
709 Nitsche, F. O., Nogi, Y., Nost, O. A., Popov, S. V., Rignot, E., Rippin, D. M., Rivera, A.,  
710 Roberts, J., Ross, N., Siegert, M. J., Smith, A. M., Steinhage, D., Studinger, M., Sun, B., Tinto,  
711 B. K., Welch, B. C., Wilson, D., Young, D. A., Xiangbin, C., and Zirizzotti, A.: Bedmap2:  
712 improved ice bed, surface and thickness datasets for Antarctica, *The Cryosphere*, 7, 375–393,  
713 doi: 10.5194/tc-7-375-2013, 2013.
- 714 ~~13.~~14. Fujita, S., Holmlund, P., Andersson, I., Brown, I., Enomoto, H., Fujii, Y., Fujita, K., Fukui,  
715 K., Furukawa, T., Hansson, M., Hara, K., Hoshina, Y., Igarashi, M., Iizuka, Y., Imura, S.,  
716 Ingvander, S., Karlin, T., Motoyama, H., Nakazawa, F., Oerter, H., Sjöberg, L. E., Sugiyama, S.,  
717 Surdyk, S., Ström, J., Uemura, R., and Wilhelms, F.: Spatial and temporal variability of snow  
718 accumulation rate on the East Antarctic ice divide between Dome Fuji and EPICA DML, *The*  
719 *Cryosphere*, 5, 1057–1081, doi:10.5194/tc-5-1057-2011, 2011.
- 720 ~~14.~~15. Greve, R., and Blatter, H. K.: *Dynamics of Ice Sheets and Glaciers*, Springer, Berlin, 2009.
- 721 ~~15.~~16. Hondoh, T., Shoji, H., Watanabe, O., Salamatin, A. N., and Lipenkov, V. Y.: Depth-age and  
722 temperature prediction at Dome Fuji station, East Antarctica, *Ann. Glaciol.*, 35, 384–390,  
723 <https://doi.org/10.3189/172756402781817013>, 2002.
- 724 ~~16.~~17. Huybrechts, P. and Oerlemans, J.: Response of the Antarctic ice sheet to future greenhouse  
725 warming, *Climate Dynamics*, 5, 93–102, 1990.
- 726 ~~17.~~18. Huybrechts, P., Rybak, O., Pattyn, F., Ruth, U., and Steinhage, D.: Ice thinning, upstream  
727 advection, and non-climatic biases for the upper 89% of the EDML ice core from a nested model  
728 of the Antarctic ice sheet, *Clim. Past*, 3, 577–589, <https://doi.org/10.5194/cp-3-577-2007>, 2007.
- 729 ~~18.~~19. Jouzel, J., Masson-Delmotte, V., Cattani, O., Dreyfus, G., Falourd, S., Hoffmann, G.,  
730 Minster, B., Nouet, J., Barnola, J. M., Chappellaz, J., Fischer, H., Gallet, J. C., Johnsen, S.,

731 Leuenberger, M., Loulergue, L., Luethi, D., Oerter, H., Parrenin, F., Raisbeck, G., Raynaud,  
732 D., Schilt, A., Schwander, J., Selmo, E., Souchez, R., Spahni, R., Stauffer, B., Steffensen, J. P.,  
733 Stenni, B., Stocker, T. F., Tison, J. L., Werner, M., and Wolff, E. W.: Orbital and Millennial  
734 Antarctic Climate Variability over the Past 800,000 Years, *Science*, 317, 793-796,  
735 <https://doi.org/10.1126/science.1141038>, 2007.

736 19-20. Kameda, T., Azuma, N., Furukawa, T., Ageta, Y. and Takahashi, S.: Surface mass balance,  
737 sublimation and snow temperatures at Dome Fuji Station, Antarctica, in 1995. *Proc. NIPR*  
738 *Symp. Polar Meteorol. Glaciol.*, 11, 24–34, 1997

739 20-21. Kameda, T., Motoyama, H., Fujita, S., and Takahashi, S.: Temporal and spatial variability of  
740 surface mass balance at Dome Fuji, East Antarctica, by the stake method from 1995 to 2006, *J.*  
741 *Glaciol.*, 54, 107–116, doi:10.3189/002214308784409062, 2008.

742 21-22. Karlsson, N. B., Binder, T., Eagles, G., Helm, V., Pattyn, F., Van Liefferinge, B., and Eisen,  
743 O.: Glaciological characteristics in the Dome Fuji region and new assessment for “Oldest Ice”,  
744 *The Cryosphere*, 12, 2413–2424, doi:10.5194/tc-12-2413-2018, 2018.

745 22-23. Kawamura, K., Parrenin, F., Uemura, R., Vimeux, F., Severinghaus, J. P., Hutterli, M. A.,  
746 Nakazawa, T., Aoki, S., Jouzel, J., Raymo, M. E., Matsumoto, K., Nakata, H., Motoyama, H.,  
747 Fujita, S., Goto-Azuma, K., Fujii, Y., and Watanabe, O.: Northern Hemisphere forcing of  
748 climatic cycles in Antarctica over the past 360,000 years *Nature*, 448, 912–917,  
749 doi:10.1038/nature06015, 2007.

750 23-24. Kawamura, K., Abe-Ouchi, A., Motoyama, H., Ageta, Y., Aoki, S., Azuma, N., Fujii, Y.,  
751 Fujita, K., Fujita, S., Fukui, K., Furukawa, T., Furusaki, A., Goto-Azuma, K., Greve, R.,  
752 Hirabayashi, M., Hondoh, T., Hori, A., Horikawa, S., Horiuchi, K., Igarashi, M., Iizuka, Y.,  
753 Kameda, T., Kanda, H., Kohno, M., Kuramoto, T., Matsushi, Y., Miyahara, M., Miyake, T.,  
754 Miyamoto, A., Nagashima, Y., Nakayama, Y., Nakazawa, T., Nakazawa, F., Nishio, F., Obinata,  
755 I., Ohgaito, R., Oka, A., Okuno, J., Okuyama, J., Oyabu, I., Parrenin, F., Pattyn, F., Saito, F.,  
756 Saito, T., Saito, T., Sakurai, T., Sasa, K., Seddik, H., Shibata, Y., Shinbori, K., Suzuki, K.,  
757 Suzuki, T., Takahashi, A., Takahashi, K., Takahashi, S., Takata, M., Tanaka, Y., Uemura, R.,  
758 Watanabe, G., Watanabe, O., Yamasaki, T., Yokoyama, K., Yoshimori, M., and Yoshimoto, T.:  
759 State dependence of climatic instability over the past 720,000 years from Antarctic ice cores and  
760 climate modeling, *Sci. Adv.*, 3, 1–13, doi:10.1126/sciadv.1600446, 2017.

761 24-25. Lilien, D. A., Steinhage, D., Taylor, D., Parrenin, F., Ritz, C., Mulvaney, R., Martín, C., Yan,  
762 J.-B., O'Neill, C., Frezzotti, M., Miller, H., Gogineni, P., Dahl-Jensen, D., and Eisen, O.: Brief  
763 communication: New radar constraints support presence of ice older than 1.5 Myr at Little Dome  
764 C, *The Cryosphere*, 15, 1881–1888, doi:10.5194/tc-15-1881-2021, 2021.

765 25-26. Lisiecki, L. E. and Raymo, M. E.: A Pliocene-Pleistocene stack of 57 globally distributed  
766 benthic  $\delta^{18}O$  records, *Paleoceanography*, 20, PA1003, doi:10.1029/2004PA001071, 2005

767 26-27. Lliboutry, L.: A critical review of analytical approximate solutions for steady state velocities  
768 and temperatures in cold ice-sheets, *Z. Gletscherkd. Glazialgeol.*, 15, 135–148, 1979

769 27-28. Martos, Y. M., Catalan, M., Jordan, T. A., Golynsky, A., Golynsky, D., Eagles, G., and  
770 Vaughan, D. G.: Heat flux distribution of Antarctica unveiled, *Geophys. Res. Lett.*, 44, 11417–  
771 11426, <https://doi.org/10.1002/2017GL075609>, 2017.

772 28-29. Motoyama H, Takahashi, A., Tanaka, Y., Shinbori, K., Miyahara, M., Yoshimoto, T., Fujii,  
773 Y., Furusaki, A., Azuma, N., Ozawa, Y., Kobayashi, K., and Yoshise, Y. : Deep ice core drilling  
774 to a depth of 3035.22m at Dome Fuji, Antarctica in 2001–07. *Annals of Glaciology*, 62, 212–  
775 222, doi:10.1017/aog.2020.84, 2021

776 29-30. Mouginit, J., B. Scheuchl, and E. Rignot: Mapping of Ice Motion in Antarctica Using  
777 Synthetic-Aperture Radar Data, *Remote Sensing*. 4. 2753-2767. doi: 10.3390/rs4092753, 2012.

778 30-31. Obase, T., A. Abe-Ouchi, F. Saito: Abrupt climate changes in the last two deglaciations  
779 simulated with different Northern ice sheet discharge and insolation, *Scientific Reports*, 11, doi:  
780 10.1038/s41598-021-01651-2, 2021



- 781 [31-32.](#) Oyabu, I., Kawamura, K., Fujita, S., Inoue, R., Motoyama, H., Fukui, K., Hirabayashi, M.,  
782 Hoshina, Y., Kurita, N., Nakazawa, F., Ohno, H., Sugiura, K., Suzuki, T., Tsutaki, S., Abe-  
783 Ouchi, A., Niwano, M., Parrenin, F., Saito, F., and Yoshimori, M.: Temporal variations of  
784 surface mass balance over the last 5000 years around Dome Fuji, Dronning Maud Land, East  
785 Antarctica, *Clim. Past*, 19, 293–321, <https://doi.org/10.5194/cp-19-293-2023>, 2023.
- 786 [33.](#) Paillard, D. Glacial cycles: Toward a new paradigm, *Review of Geophysics*, 39, 3,  
787 <https://doi.org/10.1029/2000RG000091>, 2001.
- 788 [32-34.](#) [Parizek, B. R., and Alley, R. B.: Ice thickness and isostatic imbalances in the Ross](#)  
789 [Embayment, West Antarctica: model results, \*Global and Planetary Change\*, 42, 1–4, 265–278,](#)  
790 [doi:10.1016/j.gloplacha.2003.09.005](https://doi.org/10.1016/j.gloplacha.2003.09.005), 2004.
- 791 [33-35.](#) Pattyn, F.: Antarctic subglacial conditions inferred from a hybrid ice sheet/ice stream model,  
792 *Earth. Planet. Sci. Lett.*, 295, 451–461, [doi:10.1016/j.epsl.2010.04.025](https://doi.org/10.1016/j.epsl.2010.04.025), 2010.
- 793 [34-36.](#) Parrenin, F., Barnola, J.-M., Beer, J., Blunier, T., Castellano, E., Chappellaz, J., Dreyfus, G.,  
794 Fischer, H., Fujita, S., Jouzel, J., Kawamura, K., Lemieux-Dudon, B., Loulergue, L., Masson-  
795 Delmotte, V., Narcisi, B., Petit, J.-R., Raisbeck, G., Raynaud, D., Ruth, U., Schwander, J.,  
796 Severi, M., Spahni, R., Steffensen, J. P., Svensson, A., Udisti, R., Waelbroeck, C., and Wolff,  
797 E.: The EDC3 chronology for the EPICA Dome C ice core, *Clim. Past*, 3, 485–497,  
798 [doi:10.5194/cp-3-485-2007](https://doi.org/10.5194/cp-3-485-2007), 2007.
- 799 [35-37.](#) Parrenin, F., and Hindmarsh, R.: Influence of a non-uniform velocity field on isochrone  
800 geometry along a steady flowline of an ice sheet, *Journal of Glaciology*, 53, 183, 612–622, [doi:](https://doi.org/10.3189/002214307784409298)  
801 [10.3189/002214307784409298](https://doi.org/10.3189/002214307784409298), 2007.
- 802 [36-38.](#) Parrenin, F., Fujita, S., Abe-Ouchi, A., Kawamura, K., Masson-Delmotte, V., Motoyama, H.,  
803 Saito, F., Severi, M., Stenni, B., Uemura, R., and Wolff, E.: Climate dependent contrast in  
804 surface mass balance in East Antarctica over the past 216 ka, *J. Glaciol.*, 36, 455–466,  
805 [doi:10.1017/jog.2016.85](https://doi.org/10.1017/jog.2016.85), 2016.
- 806 [37-39.](#) Parrenin, F., Cavitte, M. G. P., Blankenship, D. D., Chappellaz, J., Fischer, H., Gagliardini,  
807 O., Masson-Delmotte, V., Passalacqua, O., Ritz, C., Roberts, J., Siegert, M. J., and Young, D.  
808 A.: Is there 1.5-million-year-old ice near Dome C, Antarctica?, *The Cryosphere*, 11, 2427–2437,  
809 [doi: 10.5194/tc-11-2427-2017](https://doi.org/10.5194/tc-11-2427-2017), 2017.
- 810 [38-40.](#) Passalacqua, O., Ritz, C., Parrenin, F., Urbini, S., and Frezzotti, M.: Geothermal flux and  
811 basal melt rate in the Dome C region inferred from radar reflectivity and heat modelling, *The*  
812 *Cryosphere*, 11, 2231–2246, <https://doi.org/10.5194/tc-11-2231-2017>, 2017.
- 813 [39-41.](#) Passalacqua, O., Cavitte, M., Gagliardini, O., Gillet-Chaulet, F., Parrenin, F., Ritz, C., and  
814 Young, D.: Brief communication: Candidate sites of 1.5 Myr old ice 37 km southwest of the  
815 Dome C summit, East Antarctica, *The Cryosphere*, 12, 2167–2174, [doi:10.5194/tc-12-2167-](https://doi.org/10.5194/tc-12-2167-2018)  
816 [2018](https://doi.org/10.5194/tc-12-2167-2018), 2018.
- 817 [40-42.](#) Rignot, E., J. Mougnot, and B. Scheuchl: Ice Flow of the Antarctic Ice Sheet, *Science*. 333.  
818 1427–1430. [doi: 10.1126/science.1208336](https://doi.org/10.1126/science.1208336), 2011.
- 819 [41-43.](#) Rignot, E., J. Mougnot, and B. Scheuchl: MEaSURES InSAR-Based Antarctica Ice Velocity  
820 Map, Version 2. Boulder, Colorado USA. NASA National Snow and Ice Data Center Distributed  
821 Active Archive Center. [doi: 10.5067/D7GK8F5J8M8R](https://doi.org/10.5067/D7GK8F5J8M8R), 2017.
- 822 [42-44.](#) Ritz, C.: Time dependent boundary conditions for calculation of temperature fields in ice  
823 sheets. In: E. D. Waddington and J. S. Walder (Eds.), *The Physical Basis of Ice Sheet Modelling*,  
824 IAHS Publication No. 170, pp. 207–216. IAHS Press, Wallingford, UK, 1987.
- 825 [43-45.](#) Rodrigez-Morales, F. Braaten, D., Mai, H. T., Paden, J., Gogineni, P., Yan, J.-B., Abe-Ouchi,  
826 A., Fujita, S., Kawamura, K., Tsutaki, S., Van Liefferinge, B., Matsuoka, K., and Steinhage, D.:  
827 A Mobile, Multi-Channel, UWB Radar for Potential Ice Core Drill Site Identification in East  
828 Antarctica: Development and First Results, *IEEE Journal of Selected Topics in Applied Earth*  
829 *Observations and Remote Sensing*, 13, 4836–4847, 2020.
- 830 [44-46.](#) Saito, F. and A. Abe-Ouchi.: Thermal structure of Dome Fuji and east Dronning Maud Land,

831 Antarctica, simulated by a three-dimensional ice-sheet model, *Ann. Glaciol.*, 39, 433–438, doi:  
832 10.3189/172756404781814258, 2004.

833 ~~45-47.~~ Saito, F., and Abe-Ouchi, A.: Modelled response of the volume and thickness of the Antarctic  
834 ice sheet to the advance of the grounded area, *Ann. of Glaciol.*, 51, 41-48, doi:  
835 10.3189/172756410791392808, 2010.

836 ~~46-48.~~ Saito, F., Obase, T., and Abe-Ouchi, A.: Implementation of the RCIP scheme and its  
837 performance for 1-D age computations in ice-sheet models, *Geosci. Model Dev.*, 13, 5875–5896,  
838 doi:10.5194/gmd-13-5875-2020, 2020.

839 ~~47-49.~~ Saruya, T., Fujita, S., Iizuka, Y., Miyamoto, A., Ohno, H., Hori, A., Shigeyama, W.,  
840 Hirabayashi, M., and Goto-Azuma, K.: Development of crystal orientation fabric in the Dome  
841 Fuji ice core in East Antarctica: implications for the deformation regime in ice sheets, *The  
842 Cryosphere*, 16, 2985–3003, <https://doi.org/10.5194/tc-16-2985-2022>, 2022.

843 ~~48-50.~~ Seddik, H., Greve, R., Zwinger, T., and Placidi, L.: A full Stokes ice flow model for the  
844 vicinity of Dome Fuji, Antarctica, with induced anisotropy and fabric evolution, *The  
845 Cryosphere*, 5, 495–508, doi:10.5194/tc-5-495-2011, 2011.

846 ~~49-51.~~ Shakun, J. D., Lea, D. W., Lisiecki, L. E., and Raymo, M. E.: An 800-kyr record of global  
847 surface ocean delta O-18 and implications for ice volume-temperature coupling, *Earth Planet.  
848 Sc. Lett.*, 426, 58-68, doi:10.1016/j.epsl.2015.05.042

849 ~~50-52.~~ Sun, B., Moore, J. C., Zwinger, T., Zhao, L., Steinhage, D., Tang, X., Zhang, D., Cui, X., and  
850 Martín, C.: How old is the ice beneath Dome A, Antarctica?, *The Cryosphere*, 8, 1121–1128,  
851 doi:10.5194/tc-8-1121-2014, 2014.

852 ~~51-53.~~ Sutter, J., Fischer, H., Grosfeld, K., Karlsson, N. B., Kleiner, T., Van Liefferinge, B., and  
853 Eisen, O.: Modelling the Antarctic Ice Sheet across the mid-Pleistocene transition – implications  
854 for Oldest Ice, *The Cryosphere*, 13, 2023–2041, <https://doi.org/10.5194/tc-13-2023-2019>, 2019.

855 ~~52-54.~~ Sutter, J., Fischer, H., and Eisen, O.: Investigating the internal structure of the Antarctic ice  
856 sheet: the utility of isochrones for spatiotemporal ice-sheet model calibration, *The Cryosphere*,  
857 15, 3839–3860, <https://doi.org/10.5194/tc-15-3839-2021>, 2021.

858 ~~53-55.~~ Talalay, P., Li, Y., Augustin, L., Clow, G. D., Hong, J., Lefebvre, E., Markov, A., Motoyama,  
859 H., and Ritz, C.: Geothermal heat flux from measured temperature profiles in deep ice boreholes  
860 in Antarctica, *The Cryosphere*, 14, 4021–4037, <https://doi.org/10.5194/tc-14-4021-2020>, 2020.

861 ~~54-56.~~ Tsutaki, S., Fujita, S., Kawamura, K., Abe-Ouchi, A., Fukui, K., Motoyama, H., Hoshina, Y.,  
862 Nakazawa, F., Obase, T., Ohno, H., Oyabu, I., Saito, F., Sugiura, K., and Suzuki, T.: High-  
863 resolution subglacial topography around Dome Fuji, Antarctica, based on ground-based radar  
864 surveys conducted over 30 years, *The Cryosphere*, 16, 2967-2983, doi: 10.5194/tc-16-2967-  
865 2022, 2022

866 ~~55-57.~~ Uemura, R., Motoyama, H., Masson-Delmotte, V., Jouzel, J., Kawamura, K., Goto-Azuma,  
867 K., Fujita, S., Kuramoto, T., Hirabayashi, M., Miyake, T., Ohno, H., Fujita, K., Abe-Ouchi, A.,  
868 Iizuka, Y., Horikawa, S., Igarashi, M., Suzuki, K., Suzuki, T., and Fujii, Y.: Asynchrony  
869 between Antarctic temperature and CO2 associated with obliquity over the past 720,000 years,  
870 *Nat. Commun.*, 9, 961, doi:10.1038/s41467-018-03328-3, 2018.

871 ~~56-58.~~ Van Liefferinge, B. and Pattyn, F.: Using ice-flow models to evaluate potential sites of  
872 million year-old ice in Antarctica, *Clim. Past*, 9, 2335–2345, doi:10.5194/cp-9-2335-2013, 2013.

873 ~~57-59.~~ Van Liefferinge, B., Pattyn, F., Cavitte, M. G. P., Karlsson, N. B., Young, D. A., Sutter, J.,  
874 and Eisen, O.: Promising Oldest Ice sites in East Antarctica based on thermodynamical  
875 modelling, *The Cryosphere*, 12, 2773–2787, doi:10.5194/tc-12-2773-2018, 2018.

876 ~~58-60.~~ Van Liefferinge, B., Taylor, D., Tsutaki, S., Fujita, S., Gogineni, P., Kawamura, K., et al.,  
877 Surface mass balance controlled by local surface slope in inland Antarctica: Implications for ice-  
878 sheet mass balance and Oldest Ice delineation in Dome Fuji. *Geophysical Research Letters*, 48,  
879 e2021GL094966. doi:10.1029/2021GL094966, 2021.

880 ~~59-61.~~ Veres, D., L. Bazin, A. Landais, H. Toyé Mahamadou Kele, B. Lemieux-Dudon, F. Parrenin,

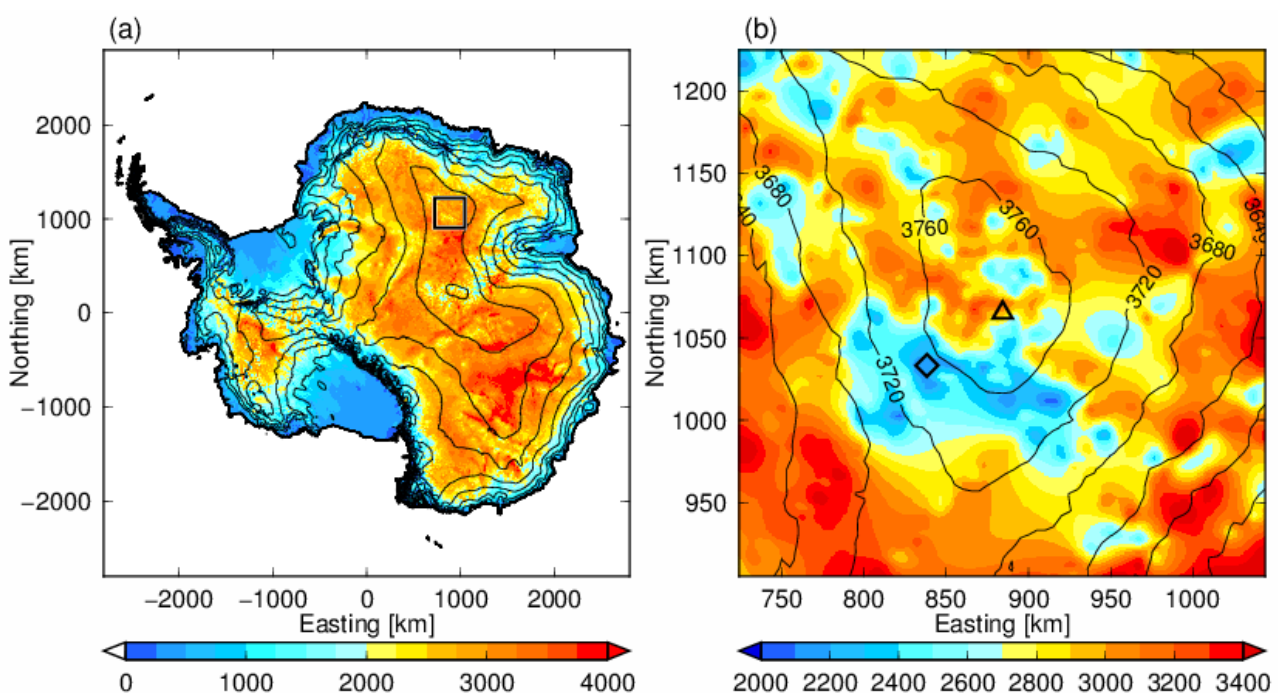
881 P. Martinerie, E. Blayo, T. Blunier, E. Capron, J. Chappellaz, S.O. Rasmussen, M. Severi, A.  
 882 Svensson, B. Vinther, and E.W. Wolff, The Antarctic ice core chronology (AICC2012): an  
 883 optimized multi-parameter and multi-site dating approach for the last 120 thousand years,  
 884 *Climate of the Past*, 9, 1733-1748, doi: 10.5194/cp-9-1733-2013, 2013.

885 ~~60-62.~~ Yamanouchi, T., Hirasawa, N., Hayashi, M., Takahashi, S., Kaneto S.: Meteorological  
 886 characteristics of Antarctic inland station, Dome Fuji, *Memoirs of National Institute of Polar  
 887 Research*. Special issue 57, 94-104, 2003

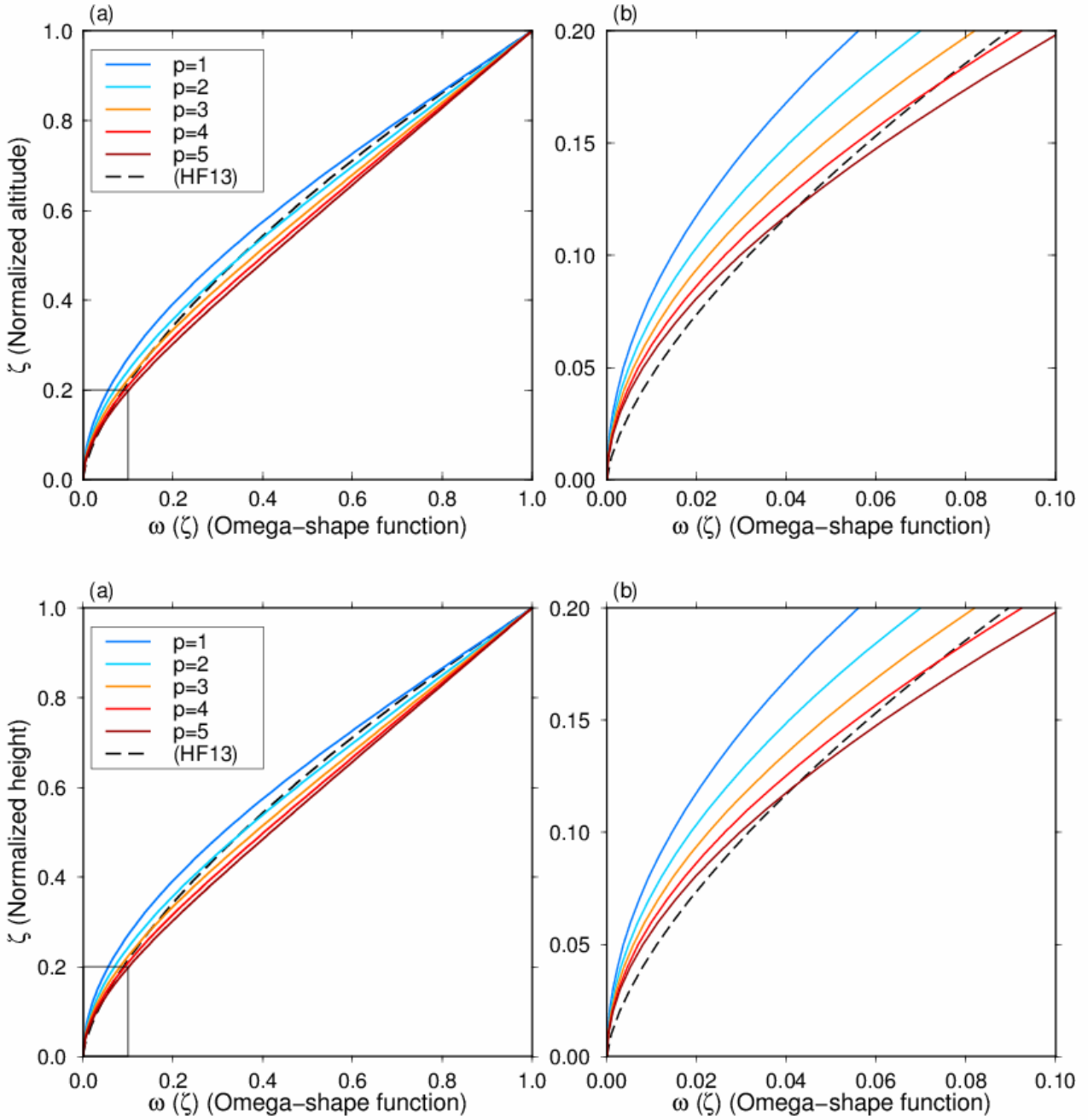
888 ~~61-63.~~ Young, D. A., Roberts, J. L., Ritz, C., Frezzotti, M., Quartini, E., Cavitte, M. G. P., Tozer, C.  
 889 R., Steinhage, D., Urbini, S., Corr, H. F. J., van Ommen, T., and Blankenship, D. D.: High-  
 890 resolution boundary conditions of an old ice target near Dome C, Antarctica, *The Cryosphere*,  
 891 11, 1897–1911, <https://doi.org/10.5194/tc-11-1897-2017>, 2017

892 ~~62-64.~~ Zhao, L., Moore, J. C., Sun, B., Tang, X., and Guo, X.: Where is the 1-million-year-old ice at  
 893 Dome A?, *The Cryosphere*, 12, 1651–1663, doi:10.5194/tc-12-1651-2018, 2018.

894



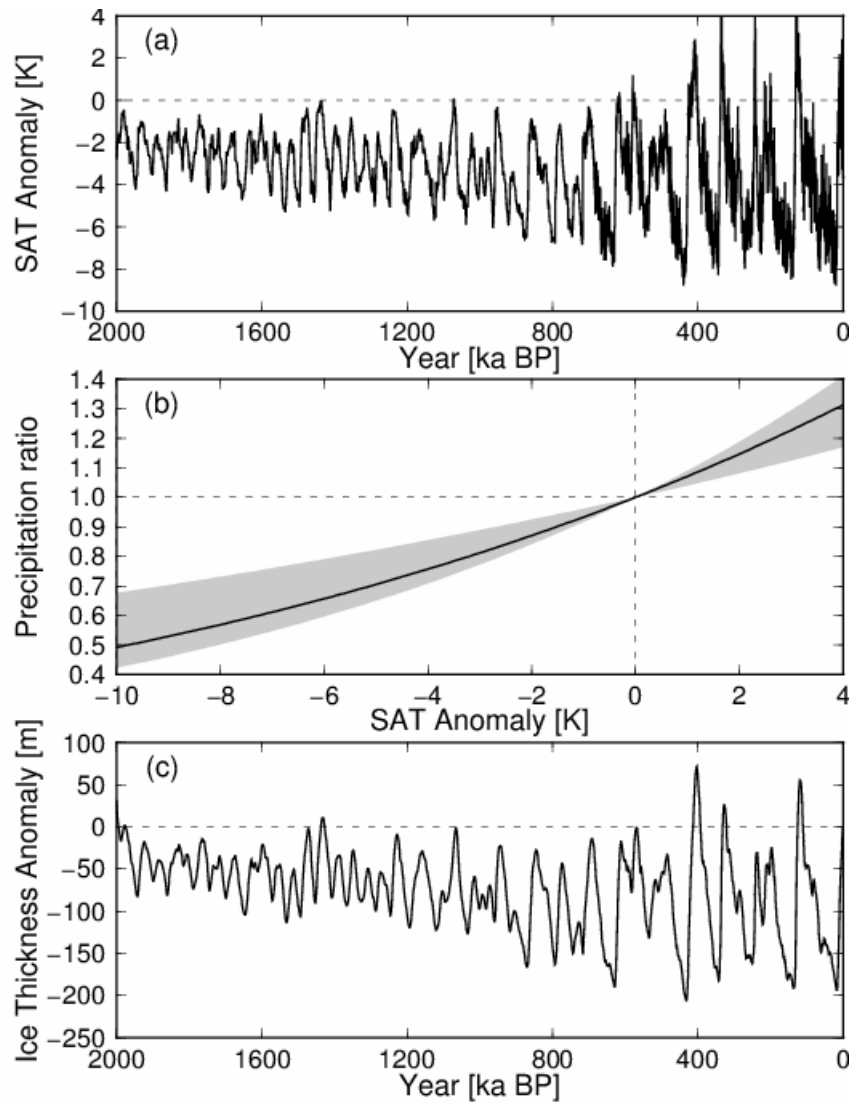
895  
 896 Fig. 1: (a) Map of Antarctica. The contours (every 500 m) indicate surface elevation, and colors  
 897 indicate ice thickness, using BEDMAP2 (Fretwell et al., 2013). The square indicates the location of  
 898 the inset shown in (b). (b) Enlarged view near DF (Dome Fuji). The triangle indicates the location of  
 899 the DF ice core site, and the diamond indicates the NDF site.



900

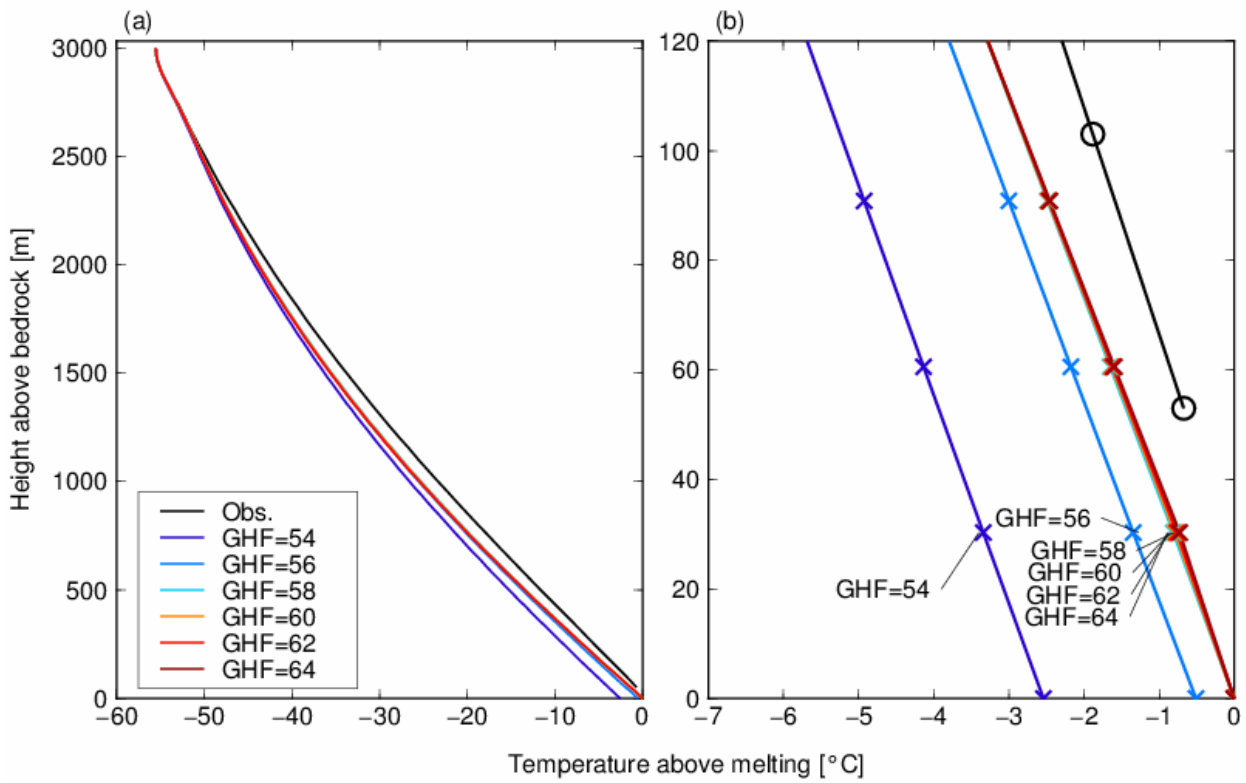
901

902 Fig. 2: (a) Normalized vertical velocity profiles adopted from Equation [3] with different  $p$   
 903 parameters. The dashed black line (HF13) indicates the vertical velocity profile used in Fischer et al.  
 904 (2013) with  $m = 0.5$ . (b) Enlarged view near the bottom of the ice column (see black rectangle in (a)).  
 905  
 906

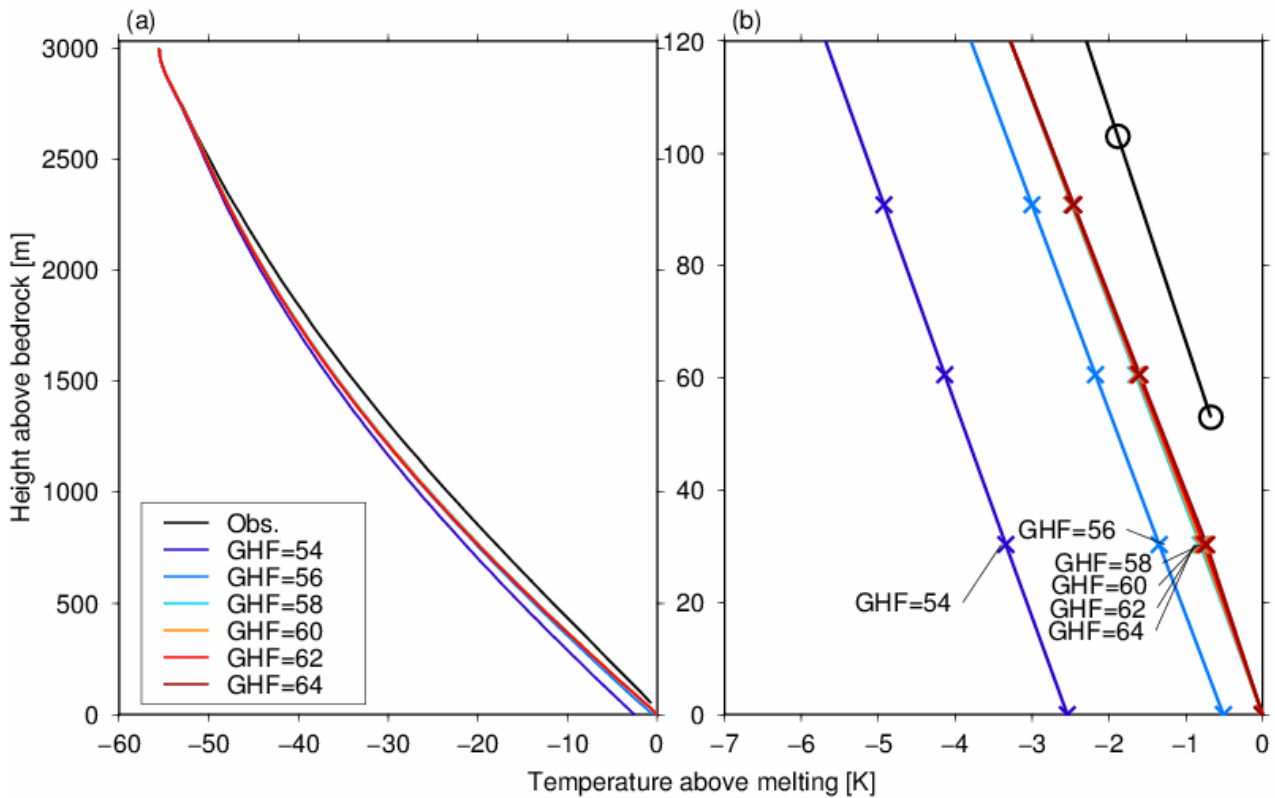


907  
 908  
 909  
 910  
 911  
 912

Fig. 3: Glacial cycle forcing used in the present study. (a) Surface air temperature (SAT) anomaly from the present day for the last 2 Ma. (b) Relationship between SAT anomaly and precipitation ratio. The black line corresponds to the relationship used in the present study; the gray shading indicates a 4%–9% increase per degree, summarized in Fox-Kemper et al. (2021). (c) Ice thickness anomaly at DF from a 3-D ice sheet model in the present study.

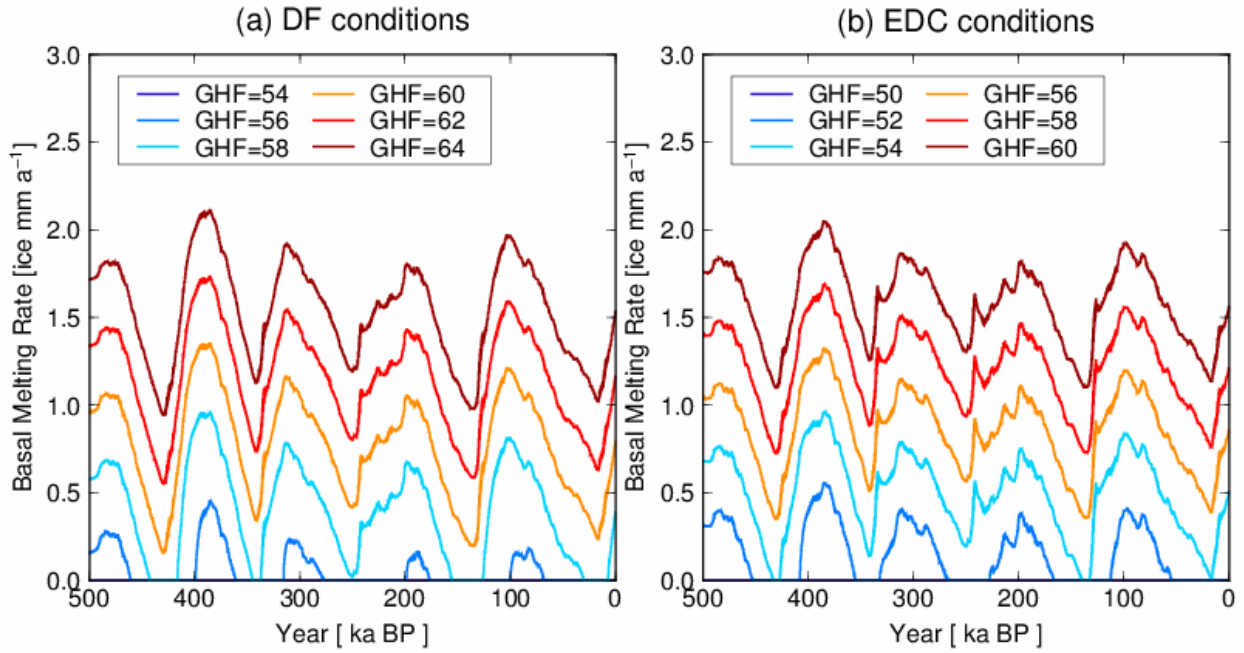


913



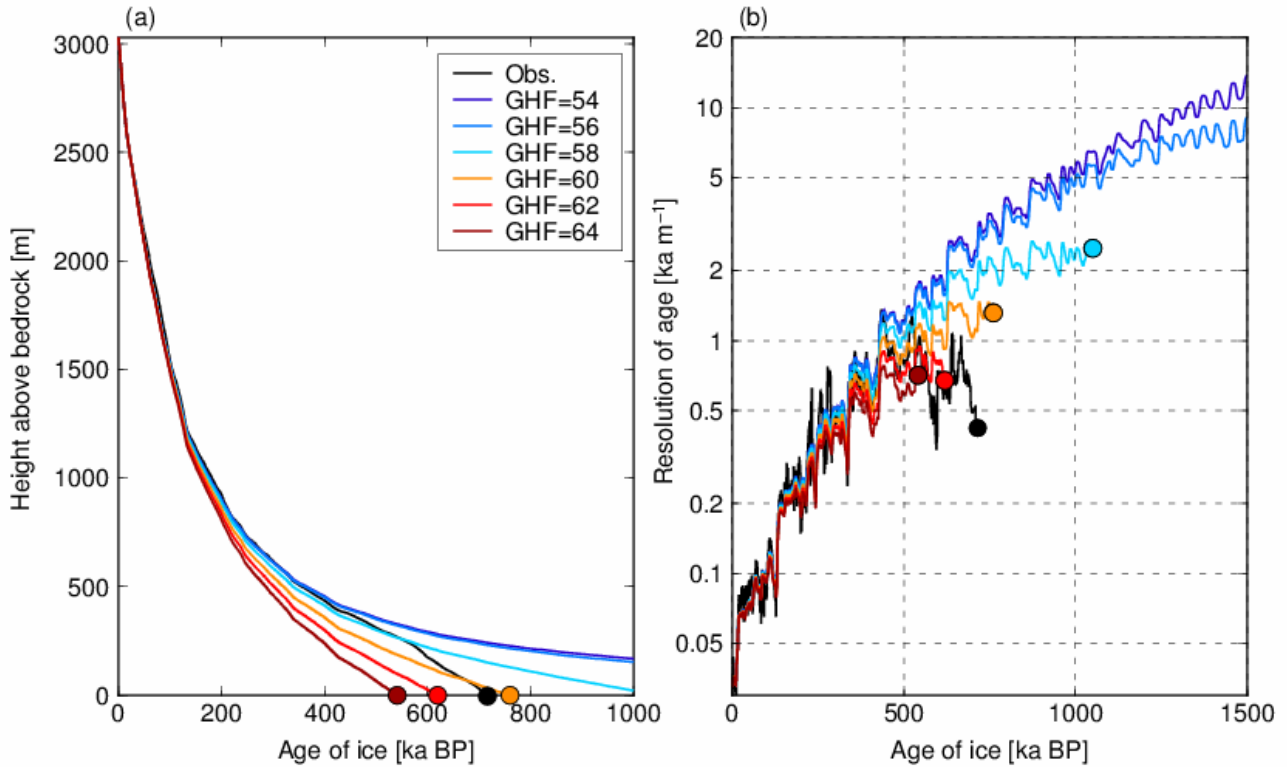
914

915 Fig. 4: Simulated vertical temperature profiles under the DF configuration (Table 1) with different  
 916 geothermal heat fluxes (GHF; units are  $\text{mW m}^{-2}$ ). (a) Simulated temperature profiles at 0 ka (end of the simulation)  
 917 from the surface to the base. (b) Close-up of (a) for the bottom 120 m of the ice column. The black lines represent the  
 918 measured temperature profiles and the black circles in (b) indicate the location of data points, while the colored  
 919 crosses in (b) represent the model grid points.



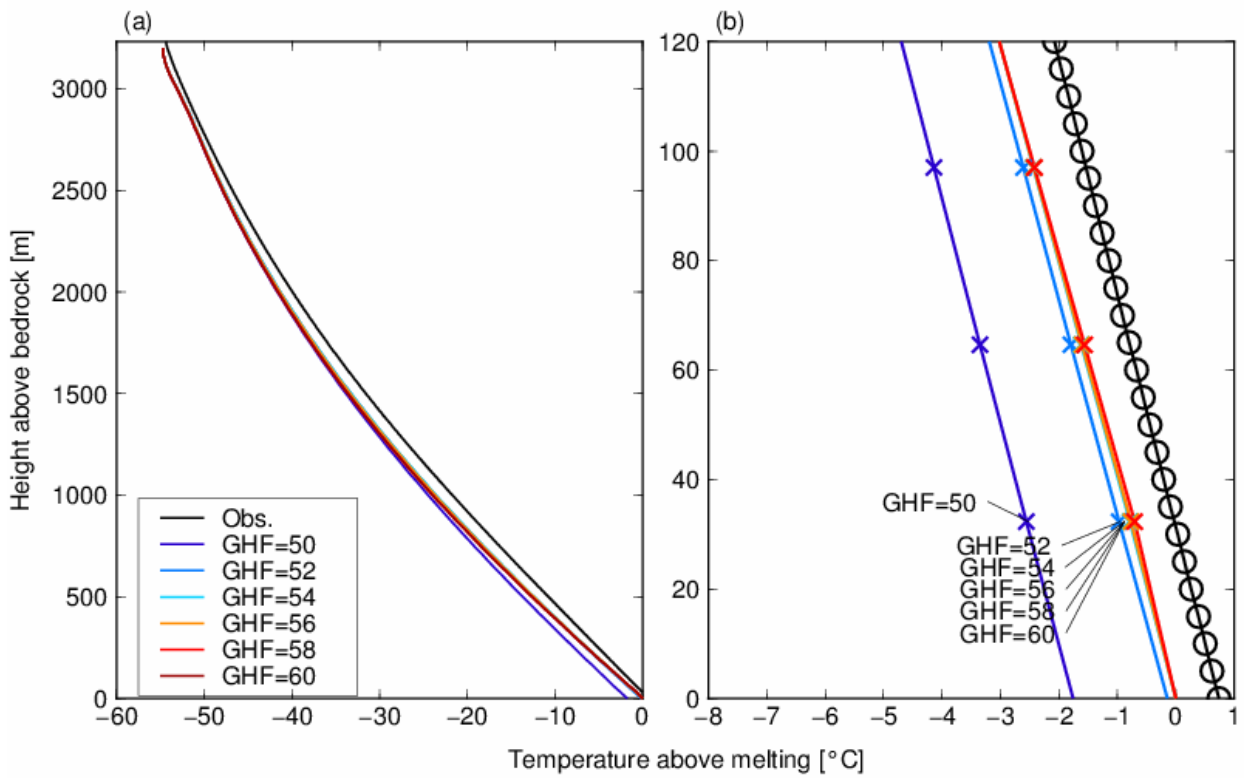
920  
921  
922

Fig. 5: Time series of the simulated basal melting rates of the last 500 ka under the DF and EDC configurations (Table 1) with different geothermal heat fluxes (GHF; units are  $\text{mW m}^{-2}$ ).

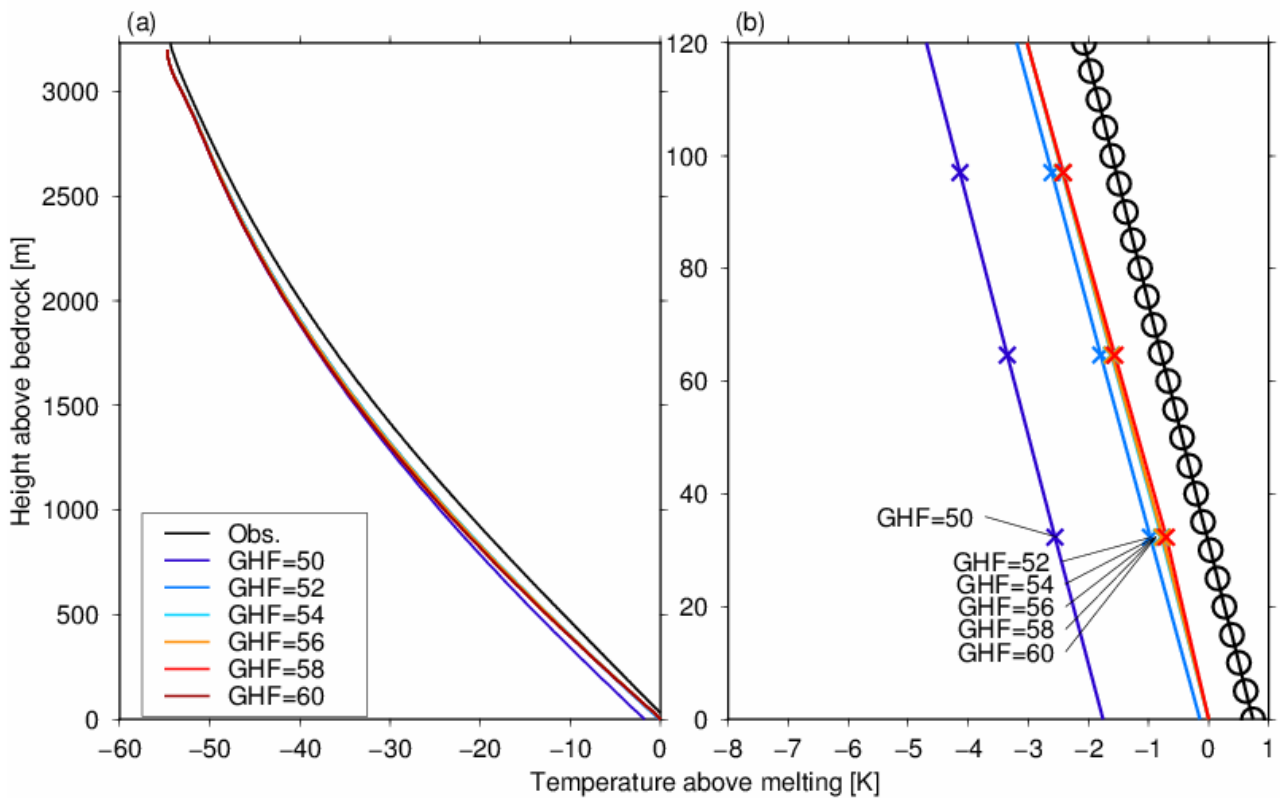


923  
924  
925  
926  
927  
928  
929

Fig. 6: Simulated vertical ice age profiles under the DF configuration (Table 1) with different geothermal heat fluxes (GHF; units are  $\text{mW m}^{-2}$ ). (a) Vertical age profiles at present (0 ka). The black line represents the reconstructed depth–age profile based on the AICC2012 chronology (Kawamura et al., 2017). The circles indicate the bottom of the ice. (b) Vertical resolution of ice age, calculated by the central difference using the simulated vertical age profiles of (a).



930



931

932

933

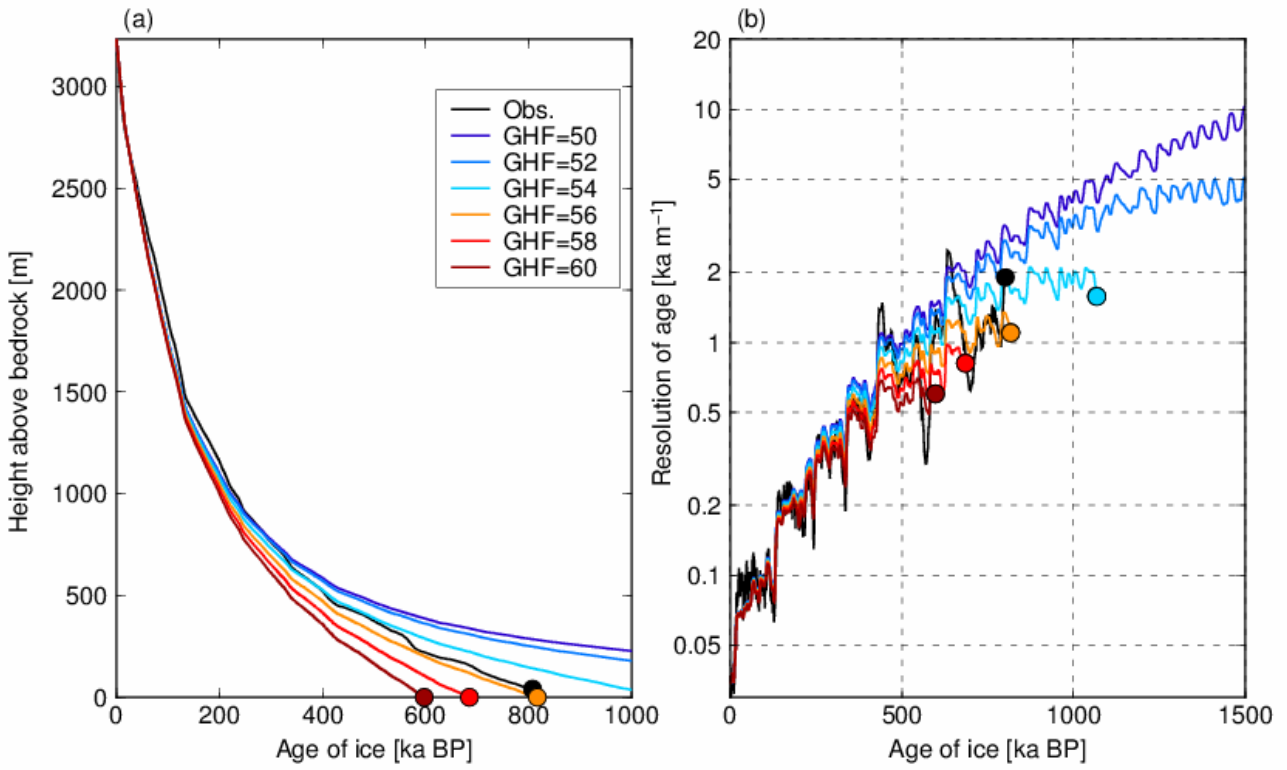
934

935

936

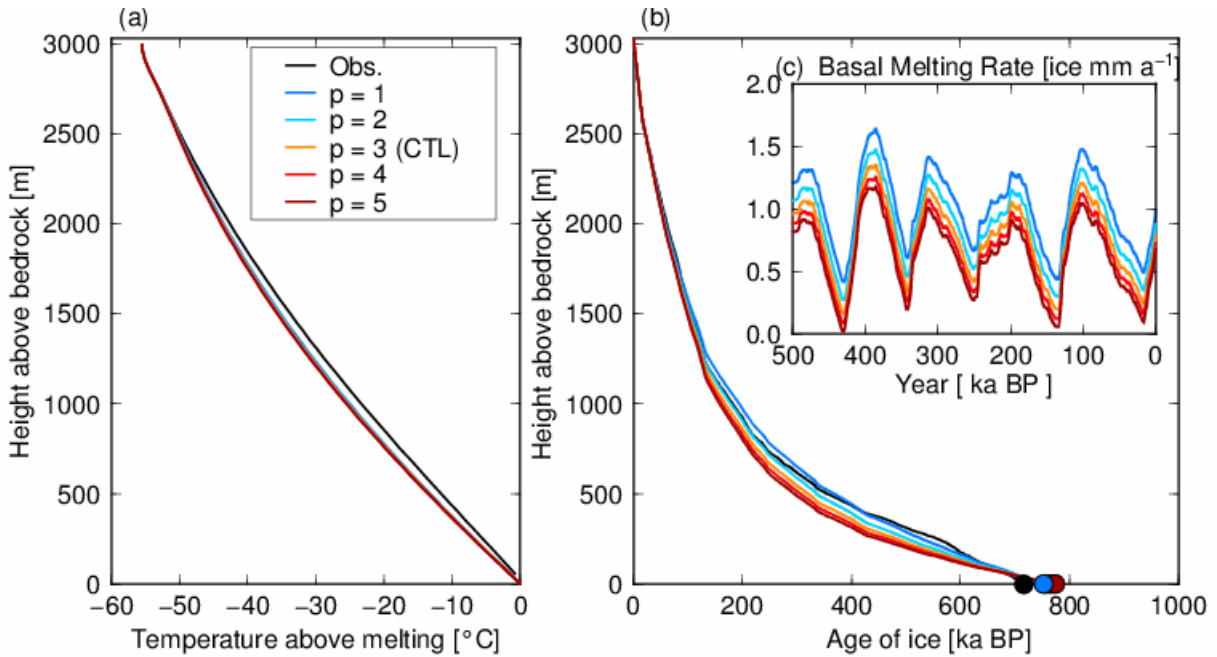
Fig. 7: Same as Fig. 4, but under the EDC configuration (Table 1) with different geothermal heat fluxes (GHF; units are  $\text{mW m}^{-2}$ ). The black lines represent the measured temperature profiles and the black circles in (b) indicate the location of data points, while the colored crosses in (b) represent the model grid points.



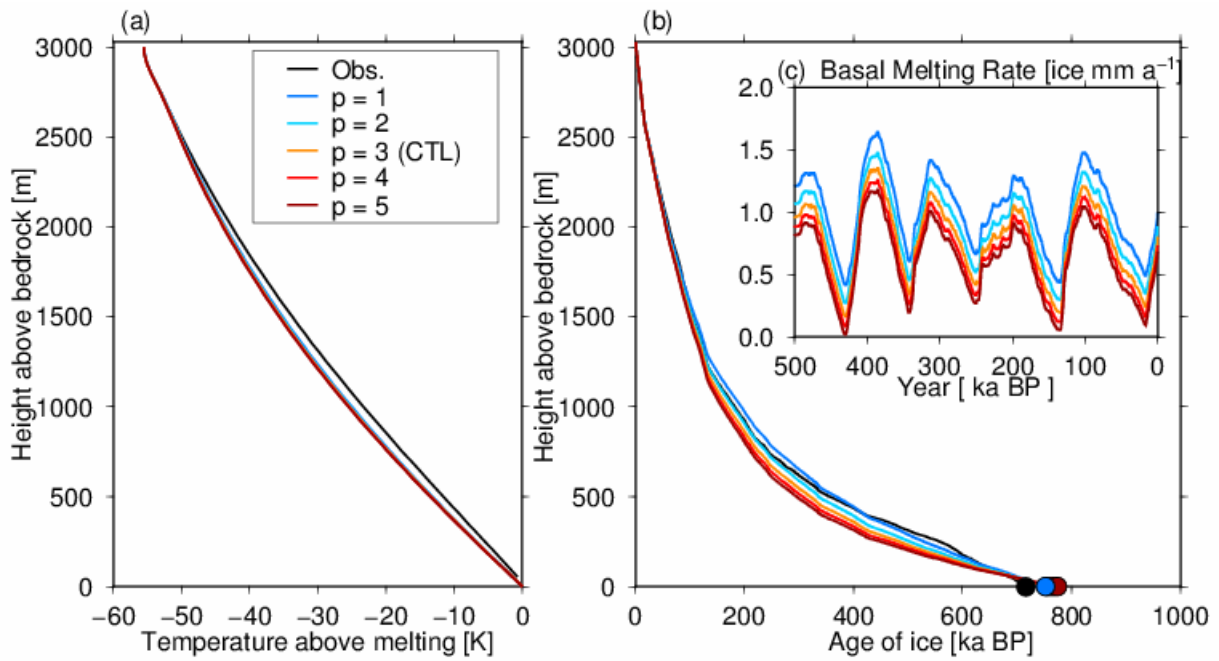


938  
939  
940  
941

Fig. 8: Same as Fig. 6, but results under the EDC configuration (Table 1). The AICC2012 chronology (Veres et al., 2013) is used in this figure for the observed depth–age profile.



942



943

944

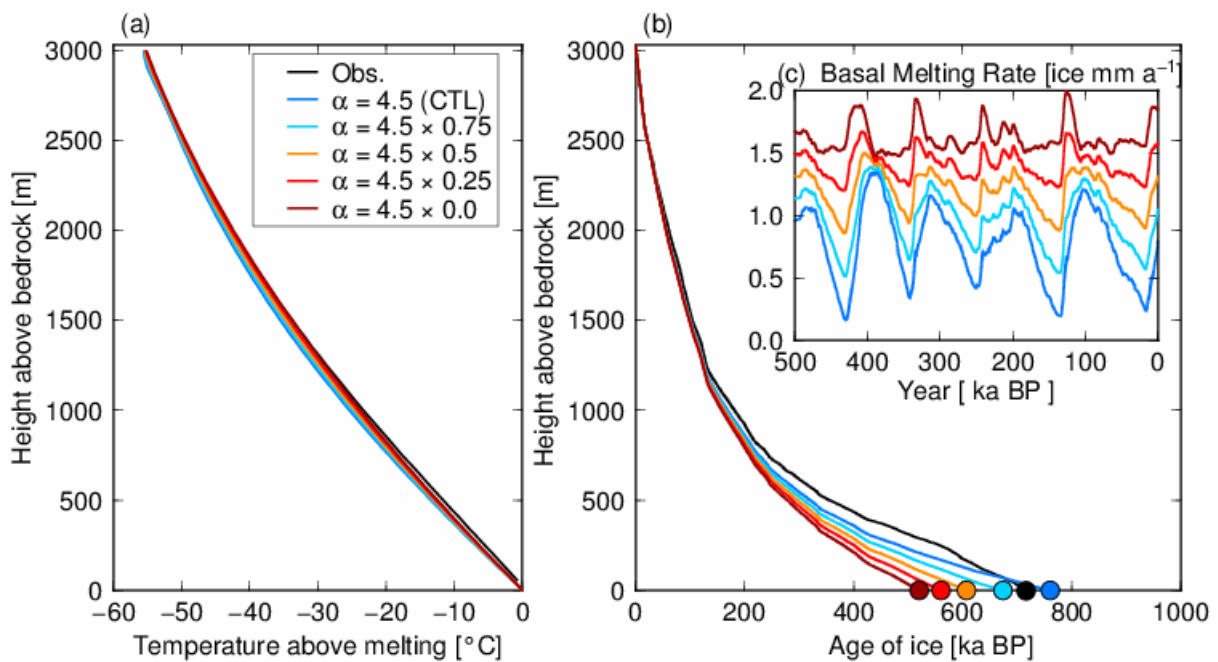
945

946

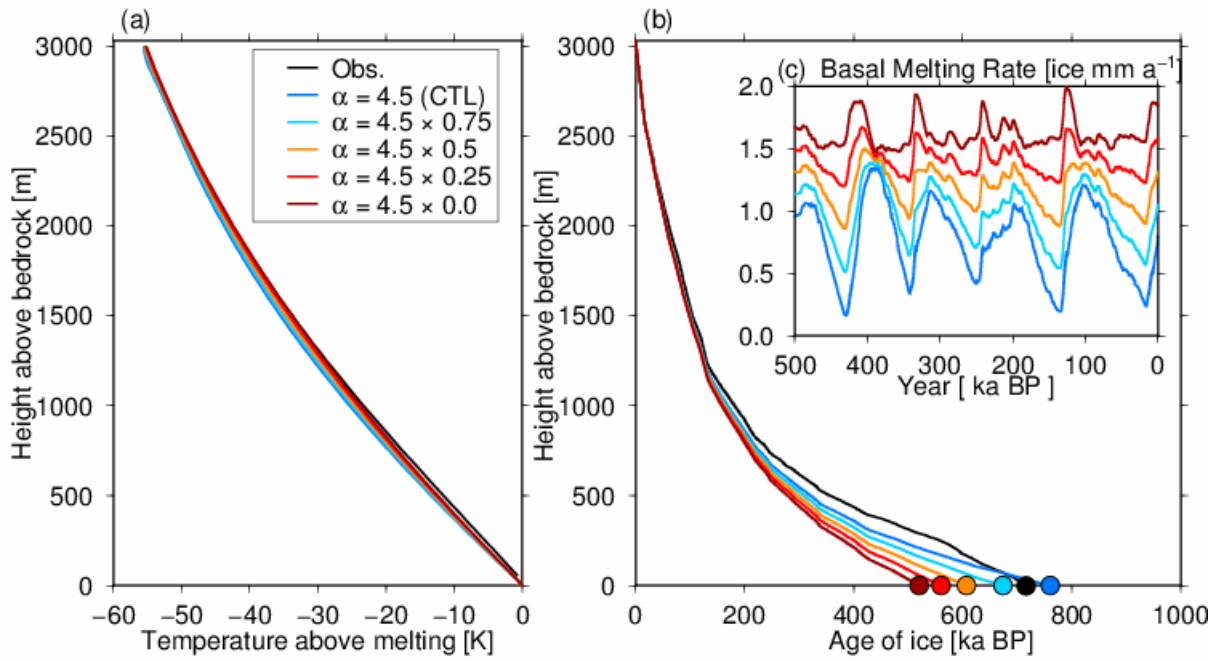
947

948

Fig. 9: Results of the DF configuration (Table 1) with different  $p$  parameters. (a) Simulated temperature profiles at present (0 ka) from the surface to the base. (b) Vertical age profiles at present (0 ka). (c) Time series of basal melting rates over the last 500 ka. A geothermal heat flux of  $60 \text{ mW m}^{-2}$  is adopted in these experiments.

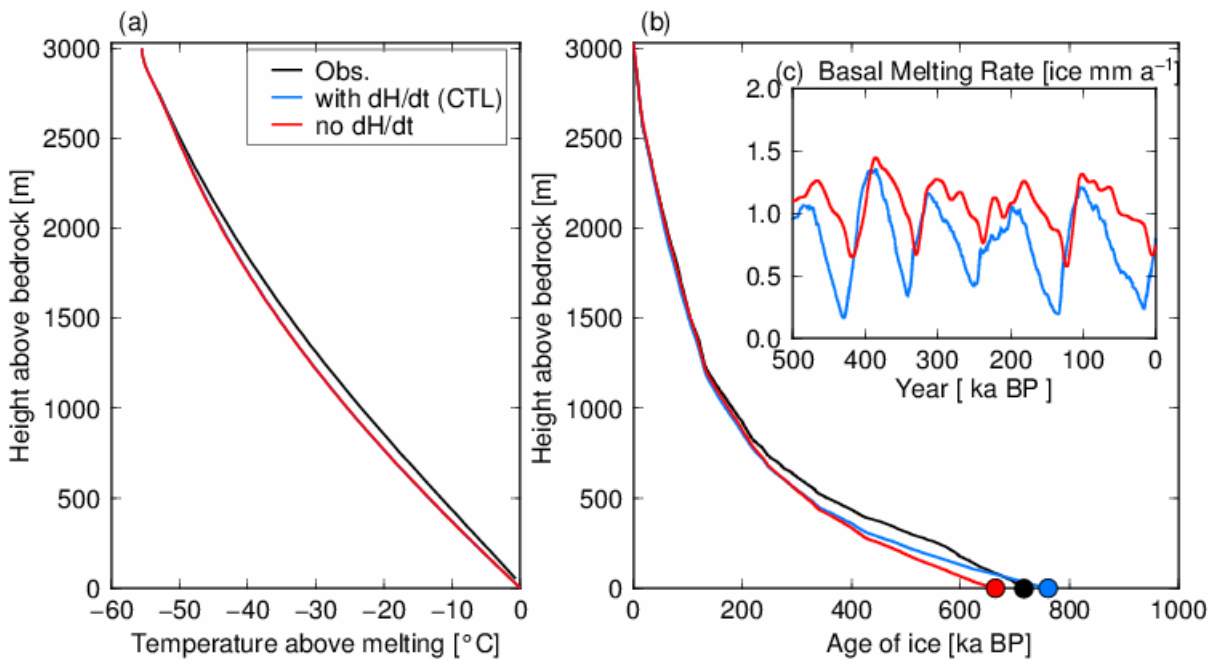


949

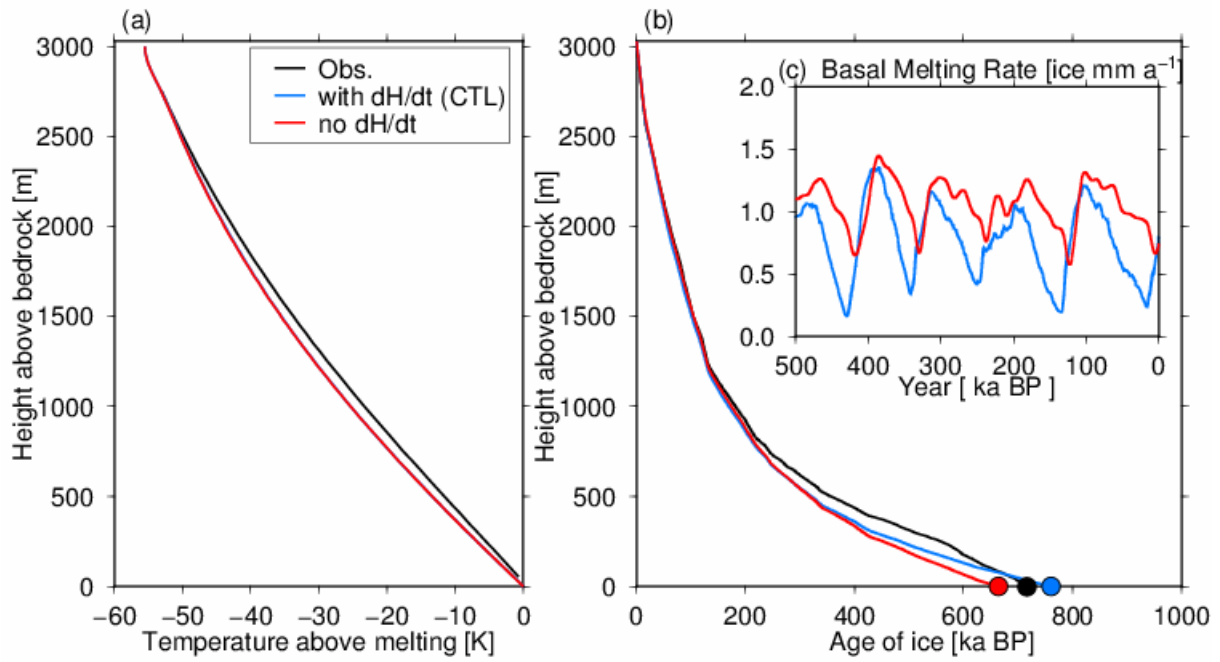


950  
951  
952  
953  
954  
955

Fig. 10: Results of the DF configuration (Table 1) with different temperature amplitudes over glacial cycles in Equation 10. A combination of  $p = 3$  and  $\text{GHF} = 60 \text{ mW m}^{-2}$  is adopted in these experiments. (a) Simulated temperature profiles at present (0 ka) from the surface to the base. (b) Vertical age profiles at present (0 ka). (c) Basal melting rates of the last 500 ka.



956



957

958

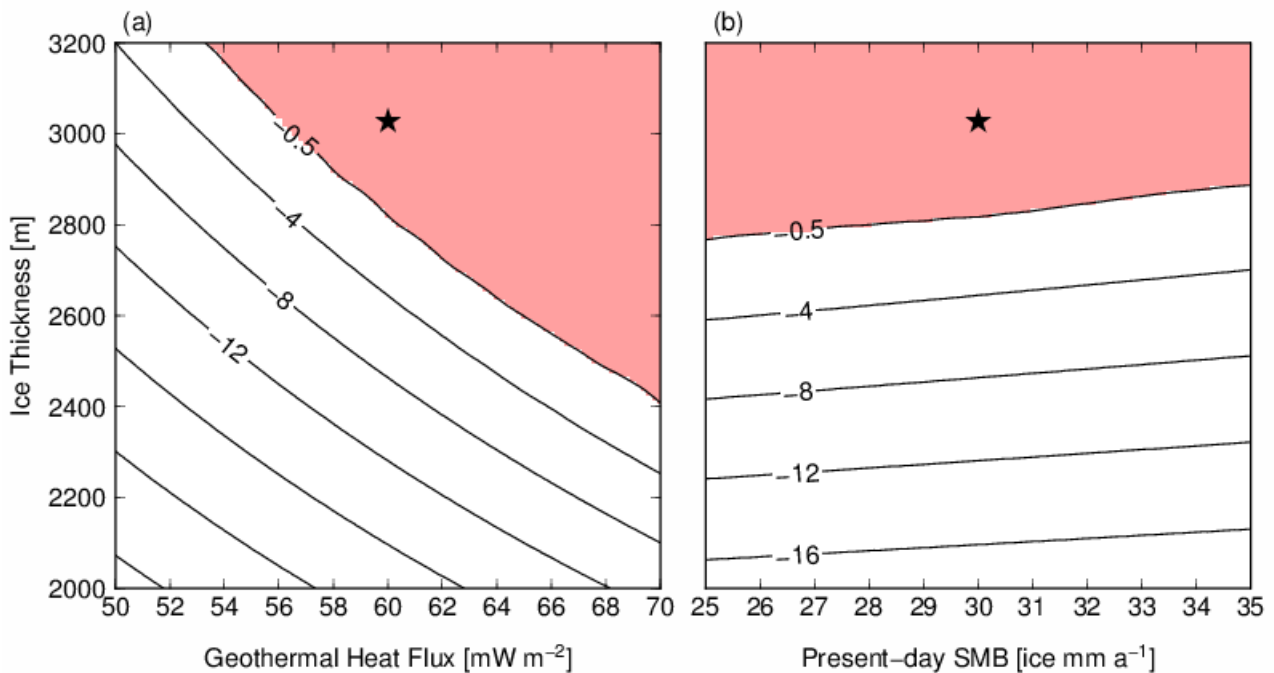
959

960

961

962

Fig. 11: Results of the DF configuration (Table 1) with and without ice thickness changes in the past. A combination of  $p = 3$  and  $\text{GHF} = 60 \text{ mW m}^{-2}$  is adopted in these experiments. (a) Simulated temperature profiles at present (0 ka) from the surface to the base. (b) Vertical age profiles at present (0 ka). (c) Basal melting rates of the last 500 ka.



963

964

965

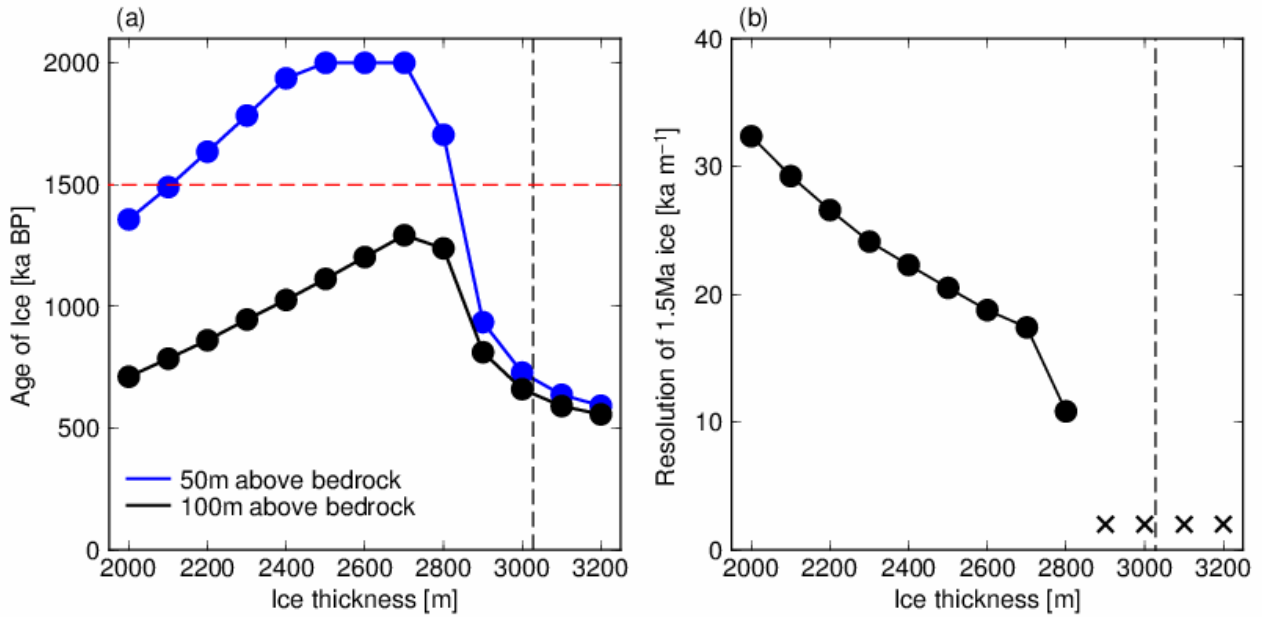
966

967

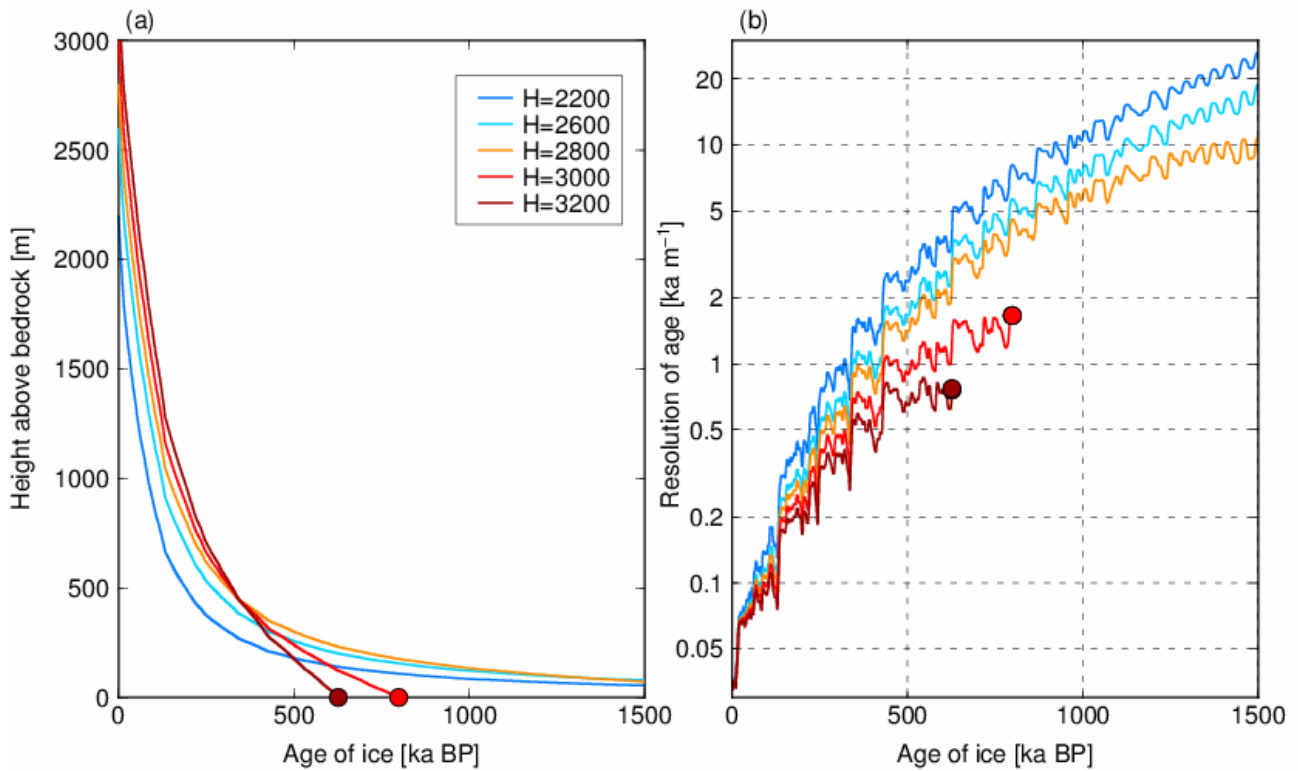
968

969

Fig. 12: Simulated basal temperature at the present day with combinations of ice thickness, geothermal heat flux, and present-day SMB. (a) Red shading indicates a basal temperature  $-0.5 \text{ }^\circ\text{C}$  below the pressure-melting point. (b) Basal temperature at the present day with  $\text{GHF} = 60 \text{ mW m}^{-2}$ . The black star represents the condition at the DF ice core ( $H = 3028 \text{ m}$ ,  $\text{SMB} = 30 \text{ ice mm a}^{-1}$ ), with a calibrated geothermal heat flux ( $60 \text{ mW m}^{-2}$ ).



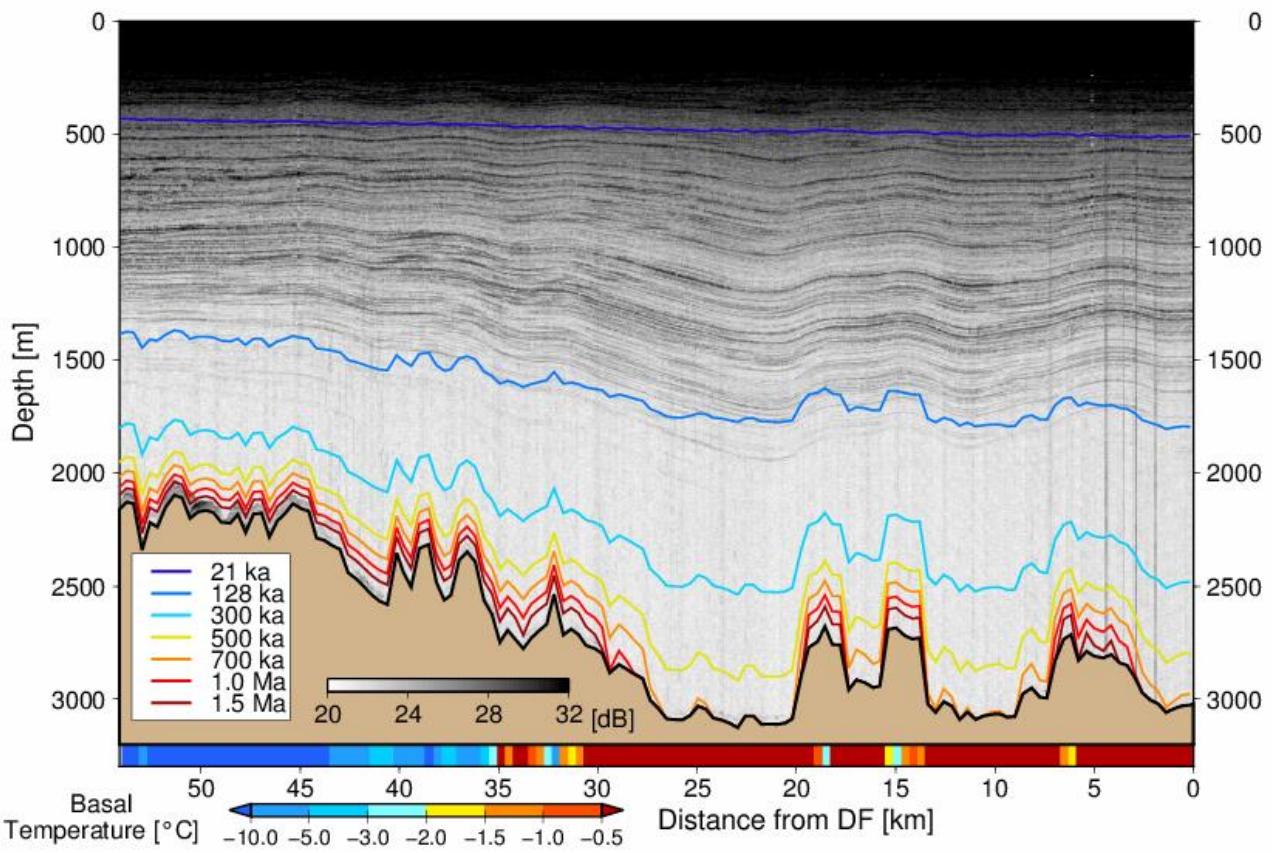
970  
 971 Fig. 13: Results with different ice thicknesses at the DF configuration (SMB = 30 ice equivalent mm  
 972 a<sup>-1</sup> and GHF= 60 mW m<sup>-2</sup>). (a) The black and blue lines indicate the simulated ages of the ice at 100  
 973 and 50 m above the bedrock, respectively. The vertical dashed line (H = 3028 m) indicates the  
 974 condition at DF, and the horizontal red dashed line indicates the age of 1.5 Ma. Note that an age of 2  
 975 Ma is the limit of the experiments. (b) The vertical axis indicates the resolution of the ice age (ka  
 976 m<sup>-1</sup>) at 1.5 Ma BP. The crosses indicate that the 1.5 Ma age of ice does not exist under these  
 977 conditions.

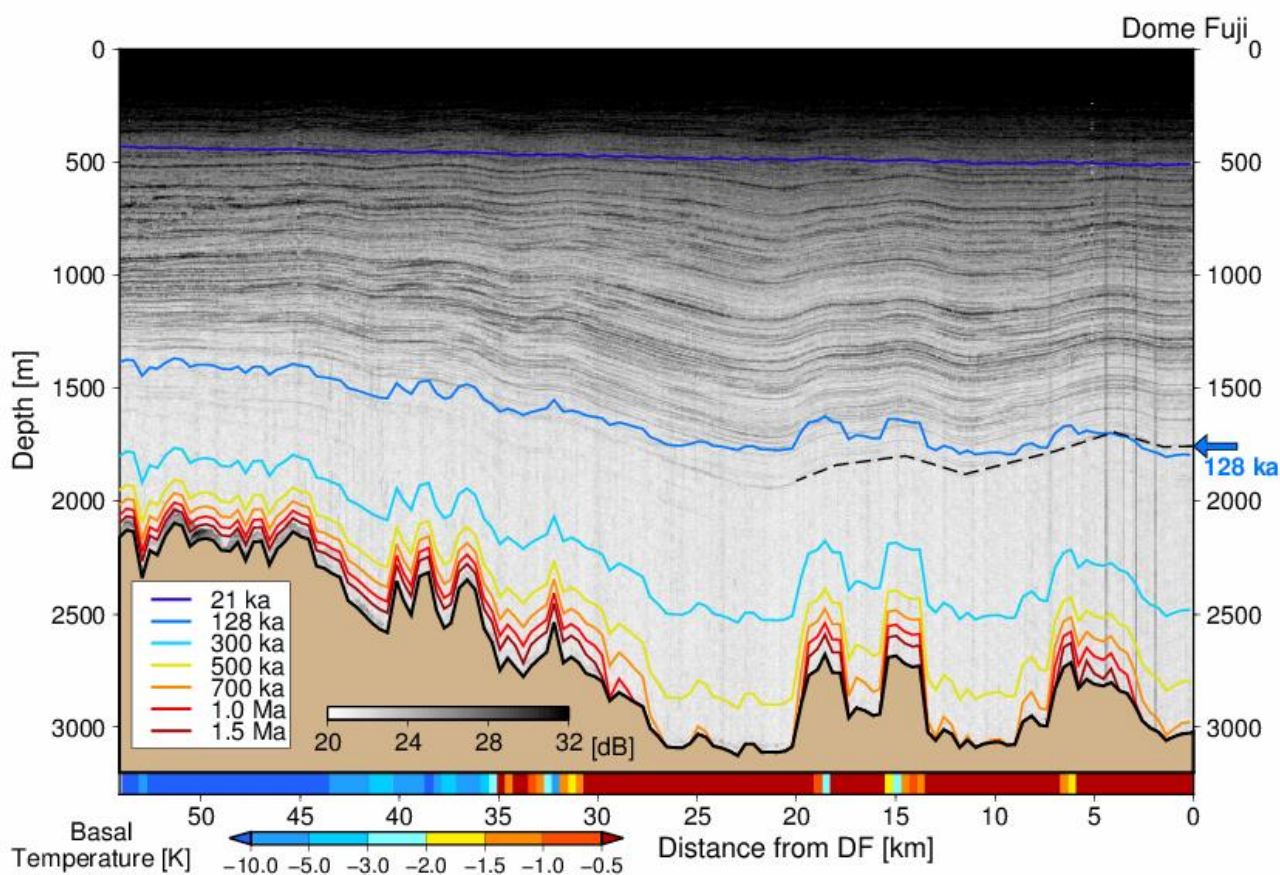


978  
 979 Fig. 14: Results with different ice thicknesses (2200, 2600, 2800, 3000, and 3200 m) and calibrated  
 980 geothermal heat flux (60 mW m<sup>-2</sup>) and SMB (30 ice equivalent mm a<sup>-1</sup>) at DF. (a) Vertical age

981 profiles at present (0 ka). (b) Vertical resolution of the ice age.

982





984  
 985 Fig. 15: Results of the experiments overlaid with the observed radargram for the DF–NDF transect.  
 986 A combination of  $p = 3$  and  $\text{GHF} = 60 \text{ mW m}^{-2}$  is adopted in these experiments. The horizontal axis  
 987 indicates the distance from DF (km), and the vertical axis indicates the depth from the surface (m).  
 988 The gray coloring indicates the reflection intensity from the ground radar surveys, and the color  
 989 contours indicate the simulated age of the ice using the 1-D model. The black dashed line indicate  
 990 the traced isochrone horizon from DF, corresponding to ~ 128 ka. The bottom color bar indicates the  
 991 simulated basal temperature (relative to the melting point) at the present-day.